NASA TECHNICAL NOTE

NASA TN D-7900

NASA TN D-7900

ANALYSIS OF LONGITUDINAL PILOT-INDUCED OSCILLATION TENDENCIES OF YF-12 AIRCRAFT

John W. Smith and Donald T. Berry

Flight Research Center
Edwards, Calif. 93523

NATIONAL AERONAUTICS AND SPACE ADMINISTRATION • WASHINGTON, D. C. • FEBRUARY 1975

1. Report No. NASA TN D-7900	2. Government Accession No.	3. Recipient's Catalog No.
4. Title and Subtitle ANALYSIS OF LONGITUDINAL PILOT-INDUCED OSCILLATION TENDENCIES OF YF-12 AIRCRAFT		5. Report Date FEBRUARY 1975
		6. Performing Organization Code
7. Author(s) John W. Smith and Donald T. Berry		8. Performing Organization Report No. H-805
		10. Work Unit No. 766-72-02
9. Performing Organization Name and Address NASA Flight Research Center P. O. Box 273 Edwards, California 93523		11. Contract or Grant No.
		13. Type of Report and Period Covered Technical Note
12. Sponsoring Agency Name and Address National Aeronautics and Space Administration Washington, D. C. 20546		14. Sponsoring Agency Code

15. Supplementary Notes

16. Abstract

During refueling operations, where the pilot must control tightly through his primary control loop to maintain position, pilots have occasionally reported longitudinal pilot-induced oscillation (PIO) tendencies with YF-12 aircraft.

One such tendency manifests itself as a continuous small-amplitude control input near a frequency of 1 cycle per second. An infrequent but more severe PIO that results in large aircraft pitching motions has also been experienced. During one incident, normal acceleration varied from $-1g$ to $3g$ at a frequency slightly higher than 0.5 cycle per second.

Aircraft flight and ground tests and simulator studies were conducted to explore these problems. Linear and nonlinear calculations of the integrated flight control system's characteristics were made to analyze and predict the system's performance and stability.

The investigations showed that the small-amplitude PIO tendency was caused by the interaction of the pilot with a combination of the aircraft's short-period poles and the structural first bending mode zeros.

The large-amplitude PIO's were triggered by abrupt corrective control actions by the pilot, which caused the stability augmentation system servo to position and rate limit. The saturation in turn caused additional phase lag, further increasing the tendency of the overall system to sustain a PIO.

17. Key Words (Suggested by Author(s)) Stability and control Pilot-induced oscillations Handling qualities YF-12 airplane	18. Distribution Statement Unclassified – Unlimited Category: 08
19. Security Classif. (of this report) Unclassified	20. Security Classif. (of this page) Unclassified	21. No. of Pages 40	22. Price* $3.00

*For sale by the National Technical Information Service, Springfield, Virginia 22151

ANALYSIS OF LONGITUDINAL PILOT-INDUCED

OSCILLATION TENDENCIES OF YF-12 AIRCRAFT

John W. Smith and Donald T. Berry
Flight Research Center

INTRODUCTION

Ever since the first manually controlled flight of powered aircraft, pilots have experienced pilot-induced oscillations (PIO) (refs. 1 and 2). Although their cause and nature differ from one aircraft to another, the problem is usually caused by the pilot's phasing his control inputs so that the aircraft's aerodynamic or control modes, or both, are amplified instead of attenuated. Two examples of longitudinal PIO's encountered with earlier production aircraft are force feedback directly to the pilot due to a bobweight (ref. 3) and force feedback through the cables and linkages on a reversible system due to control surface balances (ref. 4). More recently, nonlinear elements in stability augmentation systems (SAS) have aggravated the pilot/control system interaction problem by adding more lag, which can contribute to the pilot's initiating and sustaining an oscillation (ref. 5).

Despite the long history of PIO's, a generally valid prediction technique does not exist. One of the means available to designers for their prediction and prevention is to compare the characteristics of new aircraft with the characteristics of aircraft that have proved to be resistant or prone to these oscillations.

To contribute to the body of knowledge on aircraft PIO characteristics, this report analyzes PIO's experienced with YF-12 aircraft. Two types of PIO's have been experienced. The first, which is more common, takes place during aerial refueling when the pilot gain is high. The pilot tends to interact with the aircraft's SAS-on short-period and structural modes. This naturally makes the task more difficult, even though the attitude disturbances are not large. The second type of PIO discussed, although more infrequent, is considerably more severe in terms of aircraft rates and accelerations. Again, the PIO occurred during refueling, where pilot gain was high.

This report discusses aircraft ground and flight tests, analog simulator studies, and theoretical analyses that were made at the NASA Flight Research Center to study the phenomenon.

SYMBOLS AND ABBREVIATIONS

Physical quantities in this report are given in the International System of Units (SI) and parenthetically in U.S. Customary Units. The measurements were taken in U.S. Customary Units. Factors relating the two systems are presented in reference 6.

A amplitude

A/C aircraft

$A/C(s)$ airplane transfer function

$A(s)$ actuator transfer function

a_n normal acceleration, g

B first bending mode

C_L lift coefficient, $\dfrac{\text{Lift}}{\bar{q}S}$

C_{L_α} lift-curve slope, $\dfrac{\partial C_L}{\partial \alpha}$, per rad

$C_{L_{\delta_e}}$ change in lift coefficient with elevator deflection, $\dfrac{\partial C_L}{\partial \delta_e}$, per rad

C_m pitching moment coefficient, $\dfrac{\text{Pitching moment}}{\bar{q}S\bar{c}}$

C_{m_α} static longitudinal stability derivative, $\dfrac{\partial C_m}{\partial \alpha}$, per rad

$C_{m_{\delta_e}}$ change in pitching moment coefficient with elevator deflection, $\dfrac{\partial C_m}{\partial \delta_e}$, per rad

$C_{m_{\dot{\theta}}}$ pitch damping derivative, $\dfrac{\partial C_m}{\dfrac{\partial \dot{\theta}\bar{c}}{2V}}$, per rad

$\bar{c}$ mean aerodynamic chord, m (ft)

$F(s)$ Laplace transfer function

2

F_s stick force, N(lb)

$\dfrac{F_s}{\theta_e}$ force per pitch error, N/rad (lb/rad)

f frequency, cps, or function

G_D describing function

G_m mechanical gearing between stick and elevator

g gravitational constant, m/sec^2 (ft/sec^2)

H total hysteresis width

$H(s)$ Laplace transfer function, feedback loop

h_p altitude, m (ft)

I_Y moment of inertia about Y-axis, N-m^2 (slug-ft^2)

$j = \sqrt{-1}$

$j\omega$ imaginary part of root

K system gain

K_B first bending moment gain

K_θ pitch attitude gain, deg/deg

$L_\alpha = \dfrac{\bar{q}S}{mV} C_{L_\alpha}$, per sec

$L_{\delta_e} = \dfrac{\bar{q}S}{mV} C_{L_{\delta_e}}$, per sec

M equivalent control power, per sec^2

M_n Mach number

$M_\alpha = \dfrac{\bar{q}S\bar{c}}{I_Y} C_{m_\alpha}$, per sec^2

3

$$M_{\delta_e} = \frac{\bar{q}S\bar{c}}{I_Y} C_{m_{\delta_e}} \text{ , per sec}^2$$

$$M_{\dot{\theta}} = \frac{\bar{q}S\bar{c}^2}{2VI_Y} C_{m_{\dot{\theta}}} \text{ , per sec}$$

m	mass, kg (slugs)
N	nonlinear element
$\bar{q}$	dynamic pressure, N/m^2 (lb/ft^2)
S	reference wing area, m^2 (ft^2)
s	Laplace transform
T	transfer function
t	time, sec
V	velocity, m/sec (ft/sec)
X	output quantity
α	angle of attack, deg or rad
γ	flightpath angle, deg or rad
$\dot{\gamma}$	rate of change of flightpath angle, rad/sec
Δ	incremental change or characteristic equation
δ_e	elevator deflection, deg or rad
δ_{e_p}	pilot elevator deflection command, deg or rad
$\delta_{e_{SAS}}$	stability augmentation system input, deg or rad
δ_{e_s}	stick deflection, deg or rad
ζ	damping ratio
θ	pitch attitude, deg or rad

θ_e	pitch attitude error, $\theta_R - \theta_o$, rad
$\dot{\theta}$	pitch rate, deg/sec or rad/sec
$\ddot{\theta}$	pitching acceleration, deg/sec^2 or rad/sec^2
σ	real part of a root, rad/sec, or root mean square
τ_θ	time constant
φ	phase angle, deg or rad
ω	frequency, rad/sec

Subscripts:

c	critical
cg	center of gravity
cl	closed loop
co	crossover
cp	cockpit location
i	initial
$inbd$	inboard
n	natural frequency
o	output
$outbd$	outboard
R	reference
$1,2,3,\ldots$	sequential calculation in the order indicated

VEHICLE DESCRIPTION

Airplane

The YF-12 airplane (fig. 1) is an advanced, twin-engine, delta-wing interceptor designed for long-range cruise at Mach numbers greater than 3 and altitudes above 24,400 meters (80,000 feet). Airplane physical characteristics are given in reference 7.
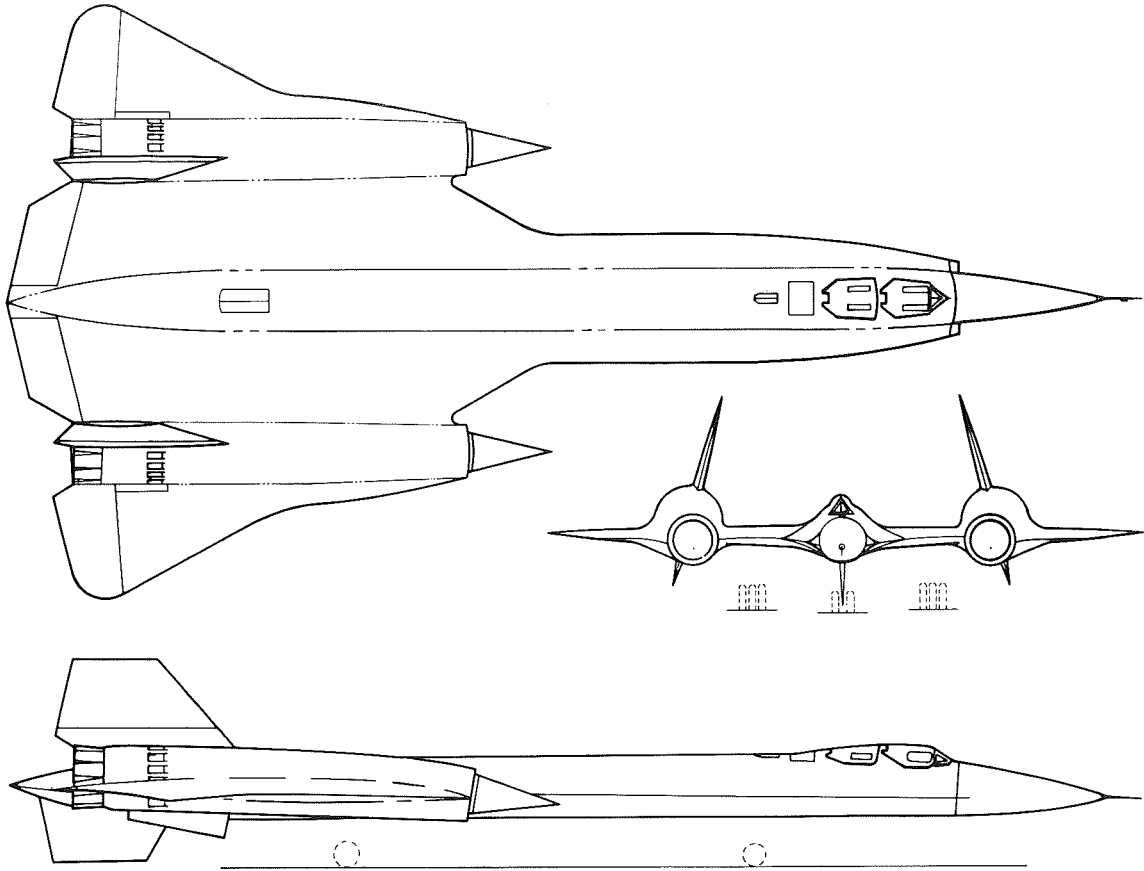
Figure 1. Three-view drawing of YF-12 airplane.

Flight Control Systems

Pilot control inputs are transferred by cables and linkages to servos in the aft section of the airplane. The inputs from the pilot and the SAS are summed in the servos that control the inboard elevon power actuators. The position of the inboard elevons is transferred by rods and linkages across the nacelles and used as an input to the servos that control the outboard elevon power actuators.

Limited-authority rate dampers are utilized in all three axes to provide the basic airplane with additional stability and damping. Damper position limits in pitch are 2.5° trailing edge up and 6.5° trailing edge down. The maximum damper surface rate is 15 degrees per second. In the feedback loop, the SAS employs gain scheduling that varies according to altitude and dynamic pressure. However, at the flight conditions of interest the gain is fixed in pitch at a value of 0.75 deg/deg/sec.

INSTRUMENTATION

Standard NASA instrumentation was used to measure the pertinent flight quantities and control positions. The sensors used to detect accelerations and angular rates were near fuselage station (F.S.) 12.7 meters (500 inches). The data were sampled at 200 times per second, conditioned, and recorded both on board and on the ground. The data were transmitted to ground stations through a pulse code modulation (PCM) system. The PCM system is considered to be accurate within 2 percent of a full-scale deflection.

ANALYSIS AND DISCUSSION

Pilot-Induced Oscillation Experiences

Aerial refueling is necessary to accomplish the design missions of the YF-12 aircraft. During the refueling maneuver the pilot must fly the aircraft to a position close to a tanker and maintain that position for several minutes. The task is demanding and requires tight, attentive attitude control on the part of the pilot. In general, as compared with other aircraft, the handling qualities of the YF-12 aircraft during refueling are considered to be good. Nevertheless, PIO tendencies during refueling have been reported. As described by the pilot, the reason for this tendency is a bobbling motion at the cockpit, which is caused by the flexing of the aircraft. The bobbling motion is benign, in that the oscillations are of small amplitude. However, the attitude changes act as triggering cues under conditions of high pilot gain and result in a coupled interaction. The interaction tendency increases as more and more fuel is taken on board the aircraft.

Figure 2 is a time history of the latter portion of a refueling maneuver. During this maneuver the control input, δ_{e_s}, was less than 3° peak to peak at a frequency of approximately 1 cycle per second. These control demands, which are somewhat annoying, are typical of the control inputs that the pilot has to make to keep the pitch excursions to a minimum. Although small, the control inputs are continuous, particularly during the final portion of the refueling maneuver, and they require additional effort on the part of the pilot.

The second type of PIO experienced is associated with large control inputs and large-amplitude responses. This type of PIO has occurred at least twice. In one instance, the PIO was triggered by an overshoot in longitudinal trim
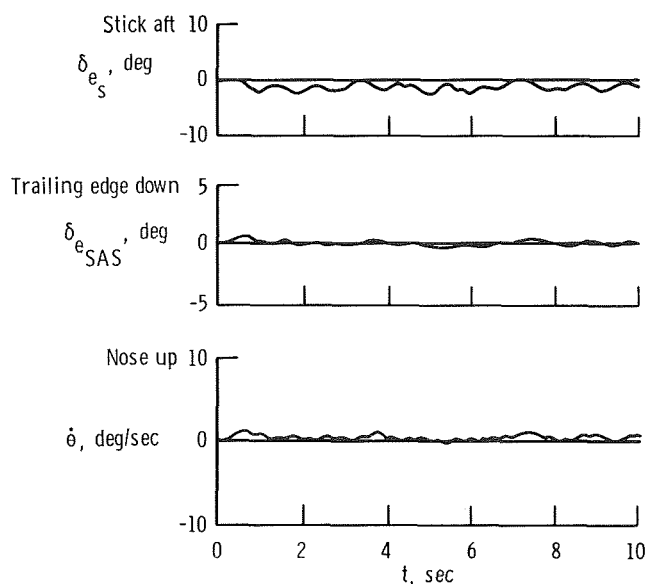

Figure 2. Time history during refueling. Typical of small-amplitude PIO tendency.

7

because of a faulty trim switch. This happened as the aircraft was approaching the tanker just before hookup. The pilot reacted normally to the trim overrun and took abrupt corrective action to keep the airplane from reaching its g limit. This caused a pitch oscillation that persisted for several cycles (fig. 3). In this particular case, the airplane's instrumentation was limited, and the only variables available are shown. It is apparent, however, that excursions of approximately $-1g$ to $3g$ occurred in normal acceleration. Control surface deflections were not recorded, but the pilot reported the incident as a definite PIO.

A study was initiated to determine the basic cause of these control difficulties.
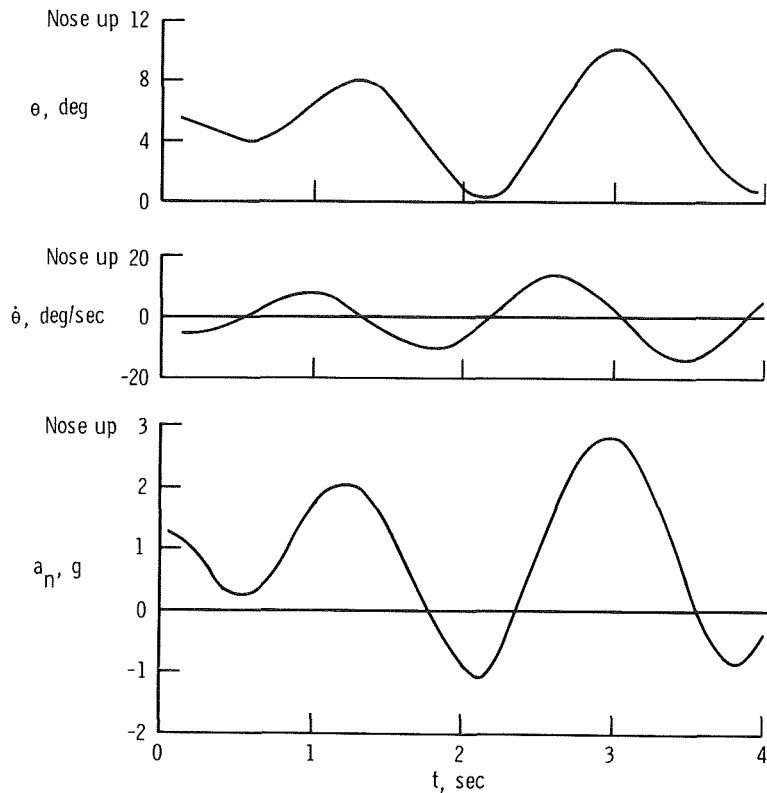
Figure 3. Large-amplitude PIO time history.

Small-Amplitude Pilot-Induced Oscillations

The PIO's experienced during aerial refueling (fig. 2) were of relatively small amplitude. Although small, such oscillations can be bothersome, because once they are excited by control activity, additional control inputs may be required on the part of the pilot to minimize them. The oscillations resulted from the coupled dynamics of both the rigid body motion and the flexing of the aircraft, and the pilot found it difficult to distinguish between the modes.

8

Because of the small amplitudes involved, linear analysis was expected to be adequate to analyze the problem. The model shown in figure 4, which shows the elements of the longitudinal control system and their relationship to the pilot, was used for the analysis. The first structural bending mode was included in the model because of the airplane's tendency to bobble and flex. In the figure, θ_o refers to the pitch angle sensed at the pilot's station, whereas θ is the rigid body pitch angle. The SAS reacts
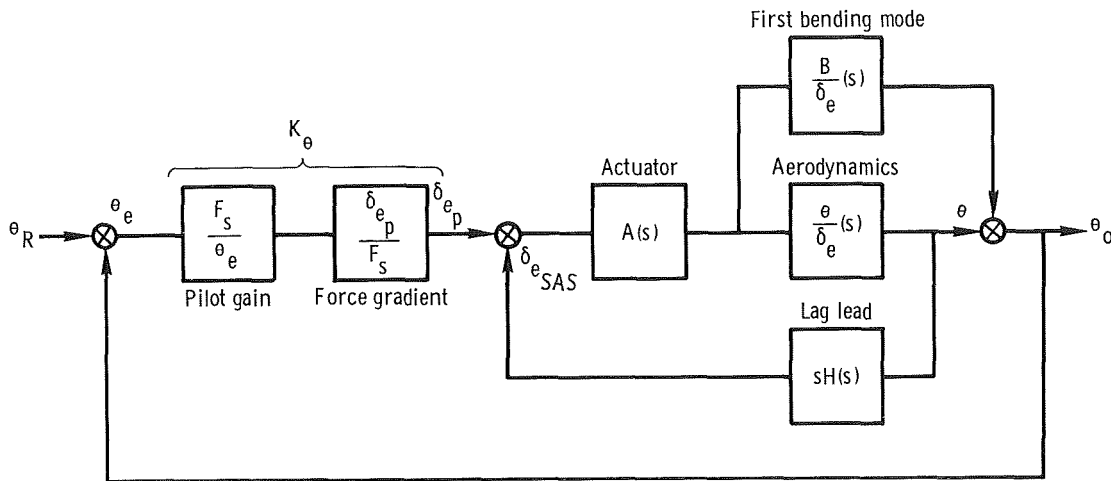
Figure 4. Linear model descriptive of longitudinal control system.

to what is essentially the rigid body pitch angle, since the system's gyroscope is on a zero slope point of the bending mode deflection curve (fig. 5, based on ref. 8).
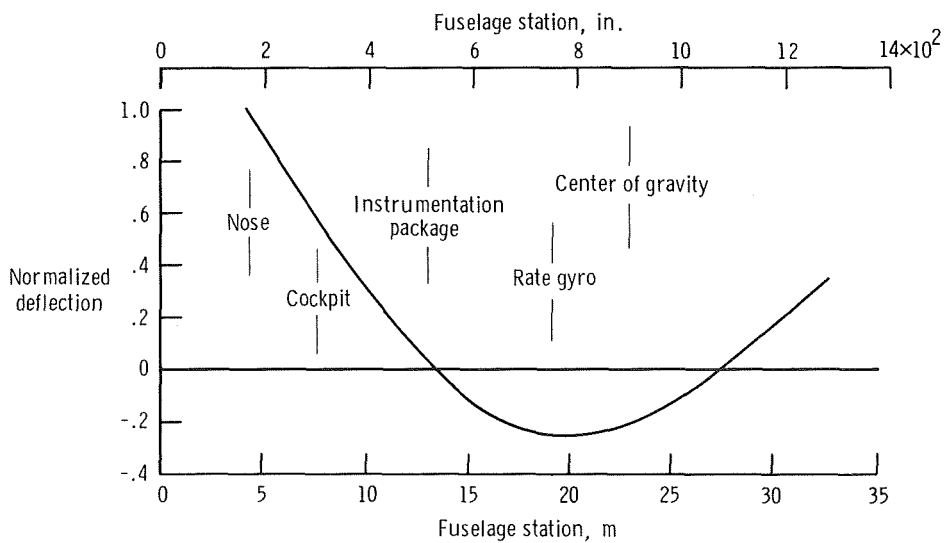
Figure 5. First structural mode shape.

Consequently, the contribution of the bending mode to pitch angle can be repre-
sented as summing downstream of the SAS feedback loop, as in figure 4. The con-
trol system's characteristics and the aerodynamics used in the analysis are de-
scribed in appendixes A to D. The poles and zeros that represent the closed-loop
or equivalent pilot-vehicle system are analyzed in linear fashion by the methods
used in reference 1 and are illustrated by the root locus in figure 6. Increasing
gain, K_θ, which is the same as increasing pilot gain, drives the poles of both the
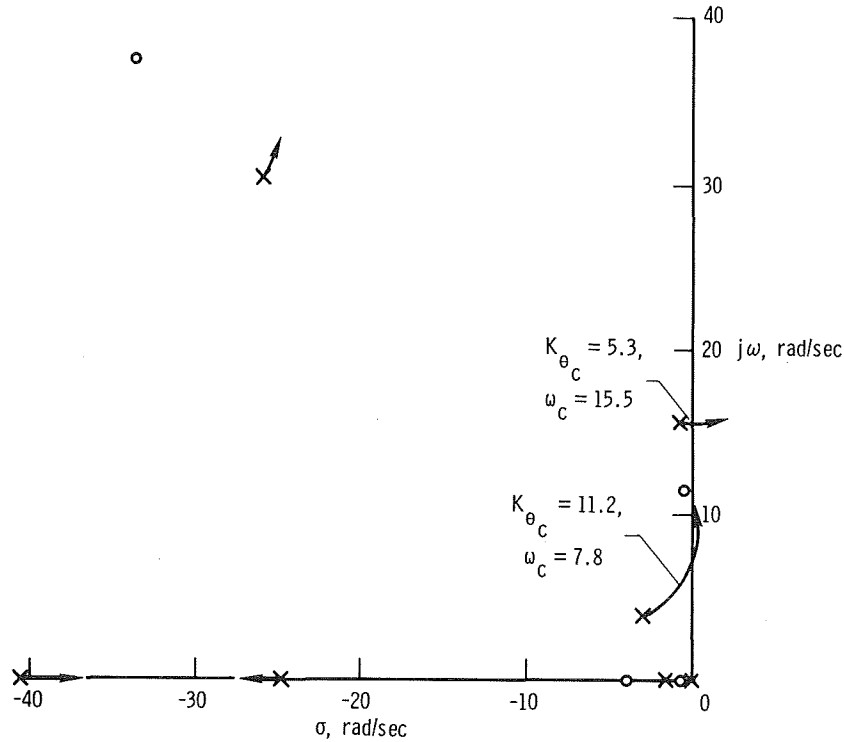
Figure 6. Root locus of longitudinal system indicating effect of increasing
gain in the attitude loop. $\dfrac{\theta_o}{\delta_{e_p}} = \dfrac{A\left(\dfrac{B}{\delta_e} + \dfrac{\theta}{\delta_e}\right)}{1 + A\dfrac{\theta}{\delta_e}sH(s)}$.

first bending and aircraft SAS-on short-period dynamics to a more oscillatory
condition. In fact, if the gain is large enough, the short-period mode would tend
toward instability near 7.8 radians per second. This depicts the less severe
small-amplitude PIO's shown in figure 2. The interaction of the pilot with the com-
bination of the airplane's SAS-on short-period mode and the structural first bend-
ing mode zeros is responsible for the added control effort during the refueling
maneuver. The root locus also indicates that the first bending mode goes unstable
at a lower pilot gain than the short-period mode. However, the frequency of the
first bending mode is far enough removed from the frequency of the pilot's control
input so that this does not happen. This was verified by random analyses like
those in figures 7 and 8 of data recorded while the airplane was connected to and
disconnected from the tanker.

10

Figures 7 and 8 show values of amplitude spectral density per cycle-per-second filter bandwidth over the pertinent frequency range. This method of analysis is discussed in reference 9. Figure 7 compares stick deflection versus frequency during refueling with stick deflection when the airplane is controlled just enough to maintain altitude. A comparison of the two curves shows that the pilot gain is
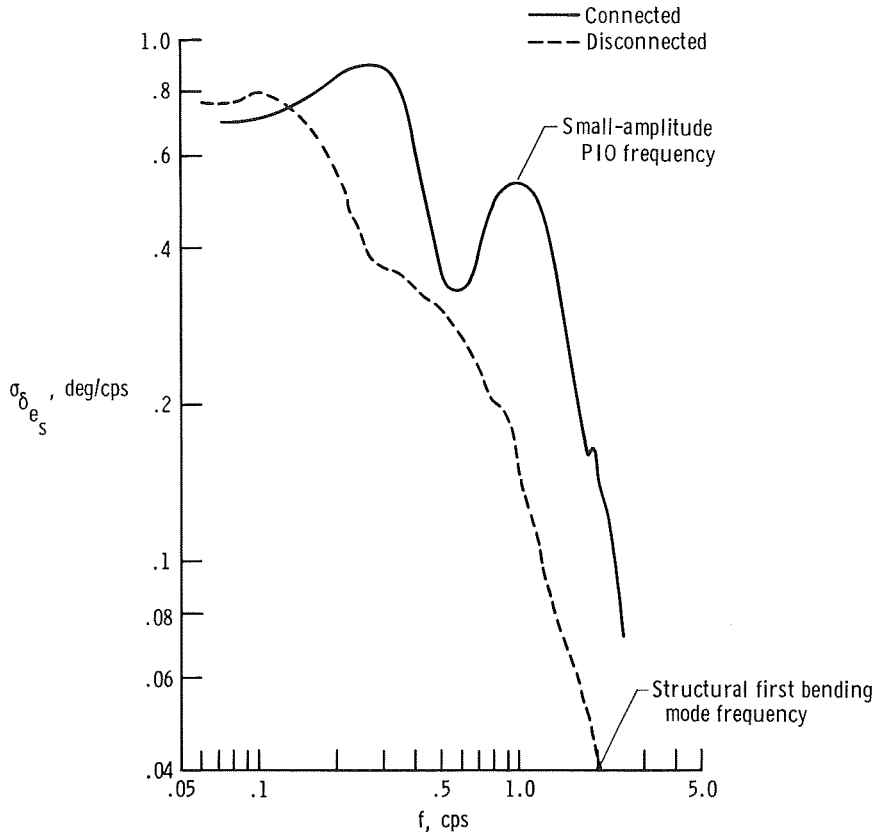

Figure 7. *Comparison of amplitude spectral density variation of primary pitch control input during flight connected to and disconnected from the tanker.*

much higher during refueling than when he is just maintaining altitude, even though the root-mean-square variation in pitch attitude is approximately the same (fig. 8). Furthermore, despite the peak in pilot input at 1 cycle per second, which is attributable to the PIO tendency, the pilot input falls off sharply at frequencies higher than 1 cycle per second (fig. 7). The 1-cycle-per-second frequency is less than one-half the frequency for the structural first bending mode (fig. 6); consequently, the pilot is unlikely to excite or sustain pure bending mode oscillations.
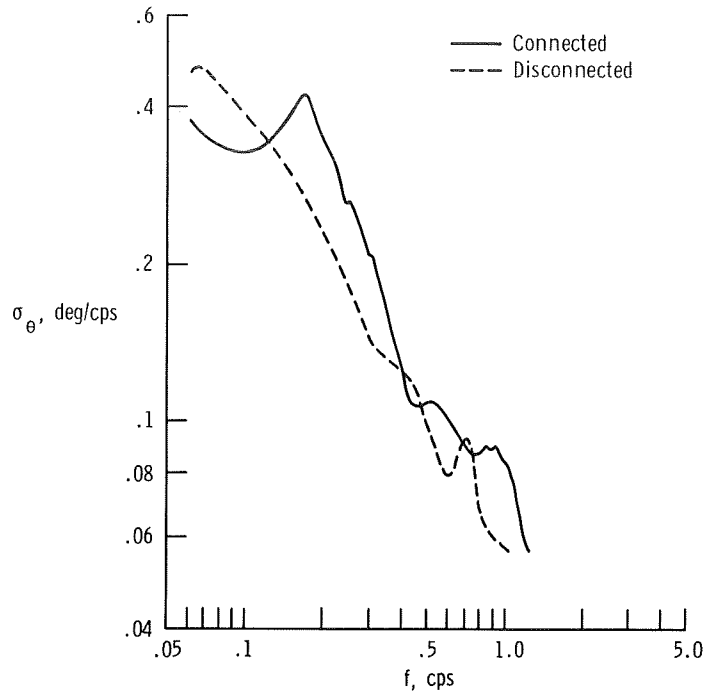
Figure 8. Comparison of amplitude spectral density variation of pitch attitude during flight connected to and disconnected from the tanker.

Large-Amplitude Pilot-Induced Oscillations

As shown in figure 3, during the large-amplitude PIO the aircraft experienced excursions of $-1g$ to $3g$ at a frequency of just over 0.5 cycle per second. This frequency is lower than predicted by linear analysis, and the magnitude of the responses suggests that the system's nonlinearities must be included in an analysis of this PIO tendency.

Although there are no control input data for the incident shown in figure 3, simulator tests, airplane closed-loop ground tests, and limited flight tests confirmed that the SAS limits were exceeded. The tests also verified the system's characteristics during PIO's (appendix A). Figure 9 shows a model of the airplane plus SAS that was derived from information obtained from the tests. The nonlinearity of the description was necessary for the analysis because of the rate and position limiting that occur in the SAS loop during a severe PIO. A digital computer program was written to give the closed-loop frequency responses of $\dfrac{\theta}{\delta_{e_p}}$ and $\dfrac{a_n}{\delta_{e_p}}$ at both the center of gravity and the cockpit, in addition to minimum boundary curves, regions,

12

and intersects for nonlinear operation. Linear conditions, which were used to make checks and comparisons, were also programed on the digital computer. (An outline of the digital computer program is presented in appendix E, along with the transfer functions used to describe the system's elements.)
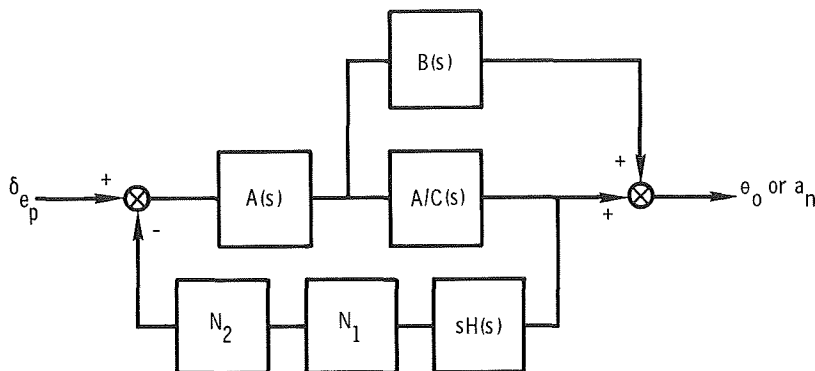

Figure 9. Model used to describe nonlinear airplane pilot open-loop longitudinal response.

Figures 10(a) and 10(b) show the results of pitch attitude response per command input versus frequency. Three calculations are presented. One is for a linear system, and the other two are for a nonlinear system. The calculations for the nonlinear system are for a control input, δ_{e_p}, of an amplitude typical of a PIO and for different damper position limits. The SAS rate limit is 12.6 degrees per second. Amplitude attenuation occurs in a normal fashion (fig. 10(a)). A comparison of the systems shows that the normal attenuation is reduced by nonlinearities, particularly near the PIO frequency, up to approximately 4 radians per second. A sizable increase in the position limits (from 2.5° to 6.5°) makes little difference in the closed-loop gain at the PIO frequency, indicating that rate limiting is the dominant influence. Above 5 radians per second, nonlinearities have virtually no effect. (The peak at 15.7 radians per second is due to structural first bending.)

Figure 10(b) shows the corresponding phase angle variation of $\dfrac{\theta_o}{\delta_{e_p}}$ versus frequency for the same three conditions. Again, nonlinearities add to the phase lag in the vicinity of the PIO frequency, and above 5 radians per second there is less difference between the three systems. The increase in phase lag and lower attenuation in the PIO frequency range would increase the tendency for PIO's.
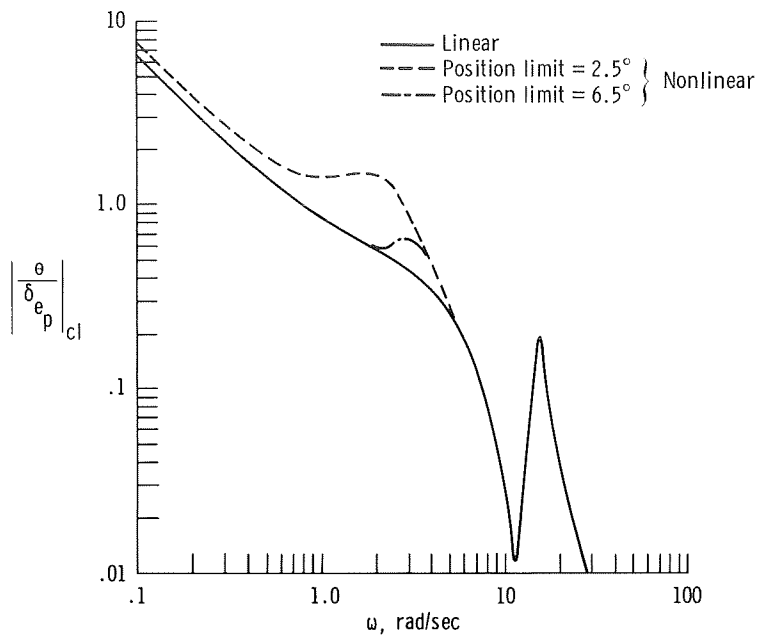
(a) Amplitude versus frequency.
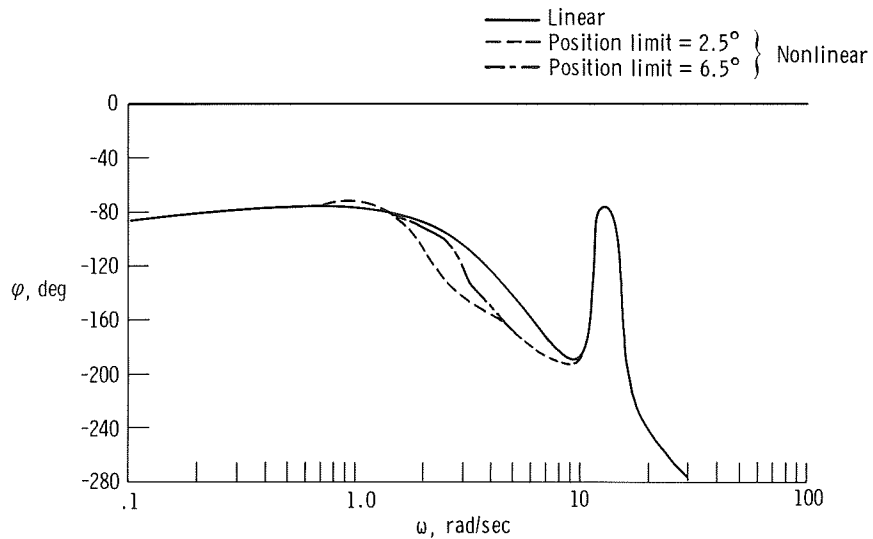
(b) Phase angle versus frequency.

Figure 10. Comparison of linear and nonlinear calculation of aircraft closed-loop pitch attitude near PIO conditions. Rate limit = 12.6 degrees per second at the cockpit; pilot loop open; $\delta_{e_p} \approx 0.1$ radian (half the peak-to-peak amplitude) for nonlinear cases.

14

Presented in figure 11 is the incremental change in normal acceleration at the center of gravity per commanded input versus frequency. The three calculations presented are those shown in figure 10. One is for a linear system and two are for a nonlinear system. The calculations for the nonlinear system are for different damper position limits and a control input, δ_{e_p}, of an amplitude typical of a PIO. The SAS rate limit is 12.6 degrees per second. The results of the calculations are compared
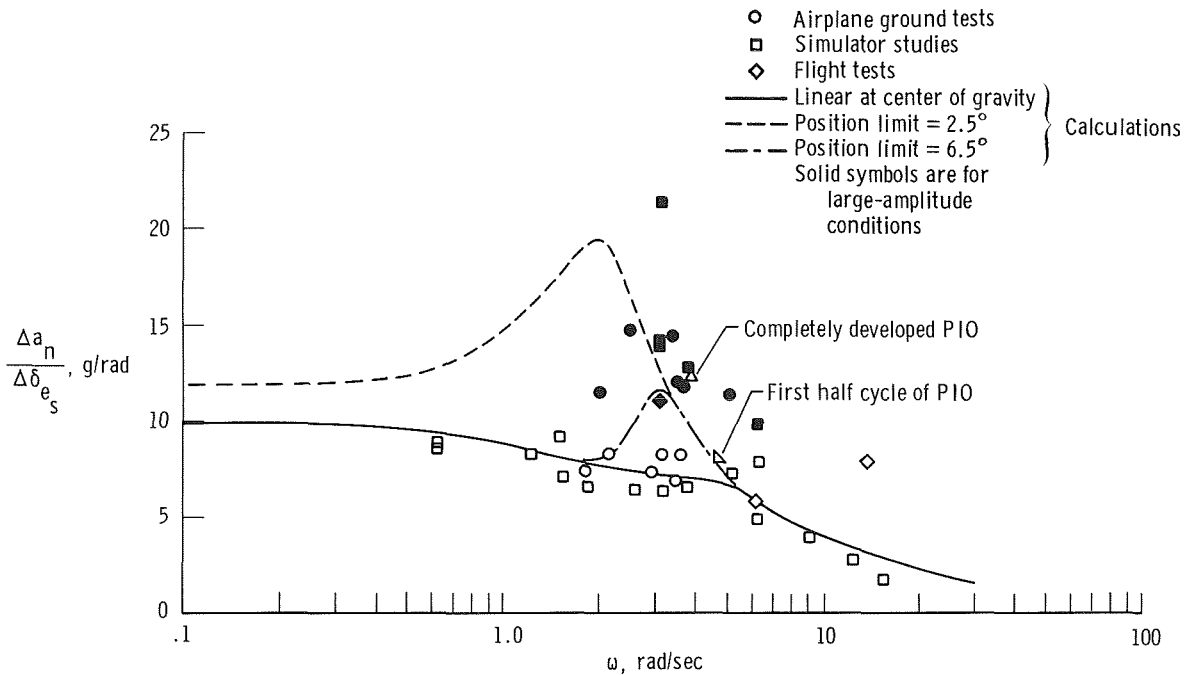

Figure 11. Comparison of experimental data with calculations of normal-force-sensitive parameter versus frequency. At the center of gravity with no body bending; SAS rate limit = 12.6 degrees per second; $\delta_{e_p} \approx 0.1$ radian (half the peak-to-peak amplitude) for nonlinear cases.

with the results of airplane ground tests, simulator studies, and flight tests. The inflight PIO's occurred at the conditions listed in table 1. The test data for the larger input amplitudes (solid symbols), most of which were obtained from ground tests and simulator studies for safety reasons, tend to peak out near a frequency of 3 radians per second. The calculated data predict a somewhat lower PIO frequency than the experimental data, probably because the experimental data were obtained for slightly different flight conditions than were assumed for the calculations. Significantly, both the calculations and the experimental data show a rise in $\dfrac{\Delta a_n}{\Delta \delta_{e_s}}$ near

the frequencies where PIO's were experienced, which means that the airplane is more responsive to control inputs in this frequency range. Aside from showing the tendency for PIO's, the comparison of the experimental data with the calculations

shows that for large input amplitudes the closed-loop nonlinear model describes the actual input-output relationship well. It also shows that at low frequencies the magnitude of position limiting has a sizable effect on the input-output relationship. At the PIO frequency (3.14 radians per second), however, the difference between the linear and nonlinear models is due primarily to rate limiting.

TABLE 1.—MAXIMUM PEAK-TO-PEAK AIRCRAFT RESPONSE AND CONTROL
INPUTS DURING PILOT-INDUCED OSCILLATIONS

(a) Flight tests

|	Pilot-induced oscillation	
	First half cycle	Completely developed
f, cps	0.75	0.61
Δa_n, g	2 (0.2 to 2.1)	4 (-1.0 to 3.0)
$\Delta \theta$, deg	4.9	10.4
$\Delta \dot\theta$, deg/sec	13.0	26.5
$\Delta \ddot\theta$, deg/sec^2	71	95

(b) Ground tests and simulator studies

	Pilot-induced oscillation			
	First half cycle		Completely developed	
	Ground tests	Simulator studies	Ground tests	Simulator studies
$\Delta \delta_e$, deg	11.5	10.6	13.4	10.4
$\Delta \delta_{e_s}$, deg	13.8	16	18.6	16
f, cps	0.80	0.80	0.61	0.56
$\left(\dfrac{\delta_{e_s}}{\delta_{e_p}}\right)_{SAS \text{ off}}$	1.47	1.46	1.66	1.46
$\Delta \delta_{e_p}$, deg	9.5	11	11.2	11

The airplane closed-loop boundaries between linear and nonlinear operation, $\delta_e = f(N_1, N_2, \omega)$, were determined by using the transfer functions descriptive of the hardware and the nonlinearities for the SAS. Figures 12(a) and 12(b) present the minimum conditions for position limits of 2.5° and 6.5°, respectively, for rate limiting of 15 degrees per second. The level of the average control input in these figures
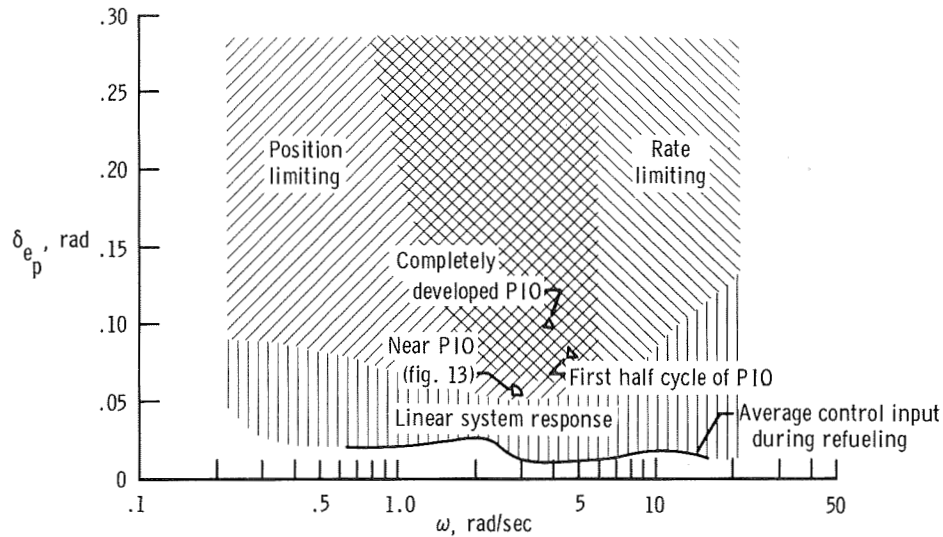
(a) Position limit = 2.5°.
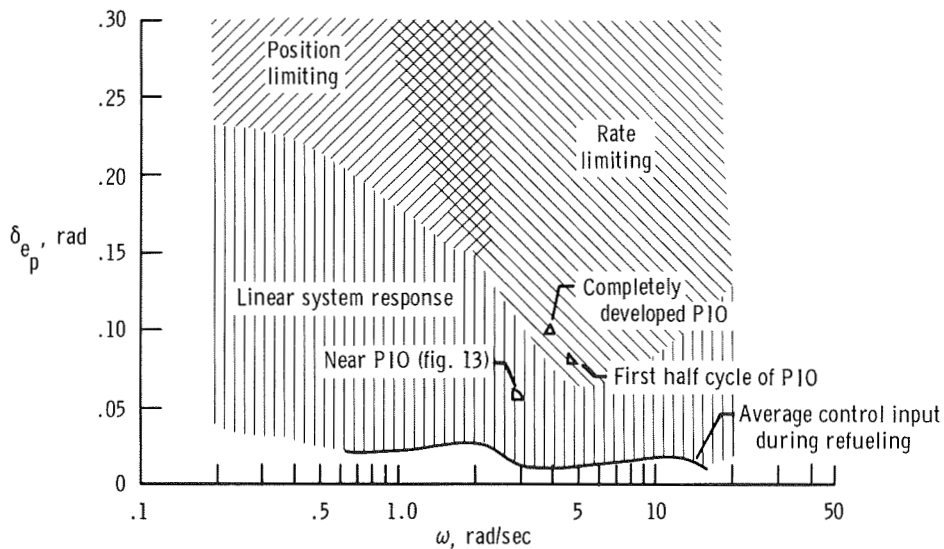
(b) Position limit = 6.5°.

Figure 12. Limiting envelopes as a function of input amplitude and frequency. Rate limit = 15 degrees per second.

was obtained from records that were taken continuously during refueling and analyzed spectrally, as previously discussed. The analysis showed that most of the time the pilot's control inputs were below the limiting boundaries. In fact, if it is assumed that there is a Rayleigh distribution for δ_{e_p}, even at the highest average input the probability that a control input will not exceed 0.05 radian is on the order of 95 percent. Therefore, it is highly unlikely that the pilot will get into a rate- or position-limiting situation. However, during the latter portion of the refueling operation (at a heavy condition) the crew has complained about a tendency toward PIO's, and on one occasion, although a PIO did not develop fully, the pilot's control input, δ_{e_s}, exceeded 7° ($t = 0$ to 2 sec, fig. 13) or $\delta_{e_p} = 0.07$ radian at a frequency of approximately 3 radians per second for two or more cycles. Figure 12 also shows the conditions under which a PIO did develop fully. The peak-to-peak values of control inputs and aircraft responses are listed in table 1. In general, for the frequency range of interest, rate limiting is more prevalent and more of a problem than position limiting.

The calculations from the digital computer program in figures 10, 11, and 12 are typical and are felt to be descriptive of the characteristics of the airframe and the augmentation system.
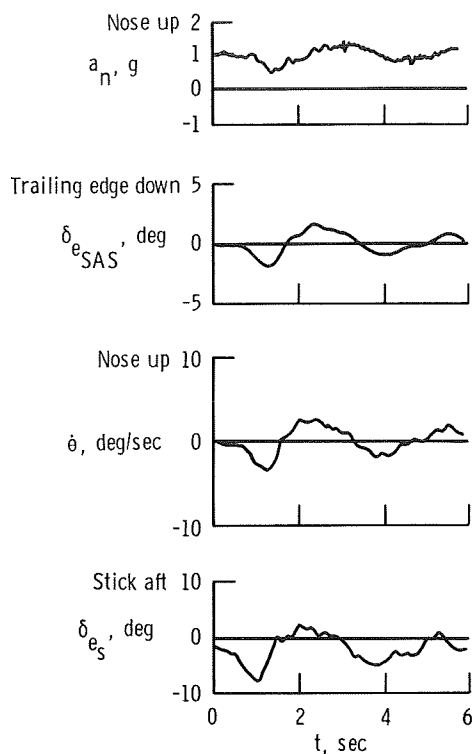

Figure 13. Time history during refueling. Typical of early part of severe PIO.

Closed-Loop Nonlinear Analysis With Pilot in the Loop

Figure 14 presents a nonlinear model of the airplane with the pilot in the loop. The nonlinearities of the artificial feel system are included in the model, as well as the nonlinearities of the SAS. As described in reference 1, a closed-loop analysis can be performed by considering the pilot to be controlling to some desired attitude, which minimizes pitch attitude error, θ_e. To sustain an oscillation in a closed-loop system, the total loop gain must be equal to 1 at a phase shift of -180°. If the pilot's adaptation during a PIO is assumed to be synchronous (in phase) with the pitch attitude error signal, $\dfrac{F_s}{\theta_e}$ can be considered a pure gain (ref. 3).
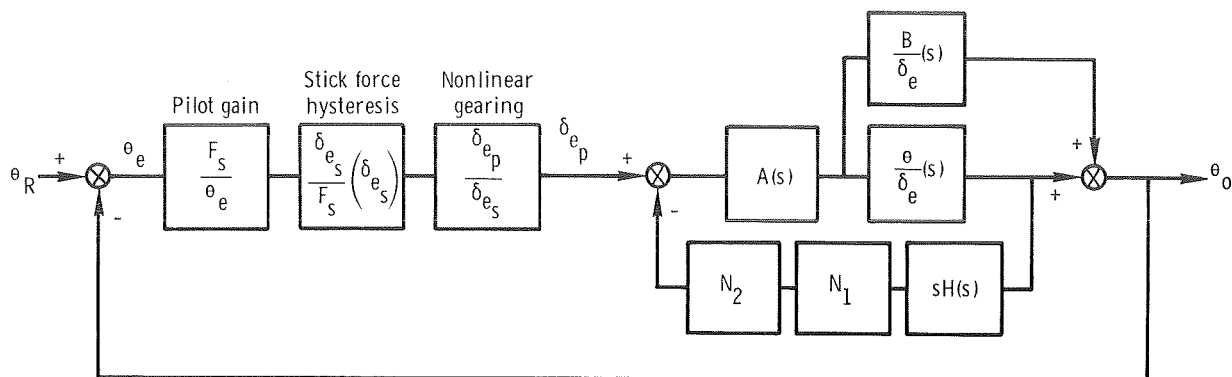
18

Figure 14. Nonlinear model of pilot-aircraft closed-loop system.

Therefore, for the PIO analysis,

$$\left(\frac{F_s}{\theta_e}\right) \text{ (Describing function) } \left[(A/C)_{cl}\right] = -1$$

where the describing function is a combination of the force hysteresis loop plus the nonlinear gearing characteristics (appendix F). Both the describing function and the transfer function of the airplane plus the SAS, $(A/C)_{cl}$, are a function of both the

frequency and initial amplitude of the pilot input, δ_{e_p}; therefore, the pilot gain required for PIO, $\dfrac{F_s}{\theta_e}$, is also a function of δ_{e_p}. Figure 15 shows the variation of PIO frequency and pilot gain as a function of input amplitude for a -180° phase shift and a total gain of 1. The PIO frequency is reduced to 50 percent to 75 percent of the linear crossover frequency (approximately 7.8 radians per second).

The conditions that triggered PIO's in flight are shown in figure 15 and described in table 1. The trend of the flight data in figure 15 is similar to the trend of the non-linear calculations, but the PIO occurred at a slightly lower frequency than predicted. As shown in the lower plot, at the PIO input amplitude (δ_{e_p} = 0.1 rad), the pilot gain necessary to sustain a PIO is only half the gain required to sustain a PIO with a linear system. Therefore, if the pilot gain was high, as during formation flight, which minimizes θ_e, a large enough control input could indeed trigger a PIO.

Such an incident as runaway or overrun trim could easily result in such an input.

It was felt that increasing the SAS rate limit to that of the servoactuator (from 12.6 degrees per second to 30 degrees per second) might alleviate the problem. Consequently, calculations were made to see what could be expected with the higher rate limit. For the condition calculated, which was near the PIO input amplitude, the pilot gain necessary to trigger a PIO with the nonlinear system was only 30 percent lower than the gain that would trigger one with a linear system. In addition,

with the higher rate limit, the PIO frequency increased to approximately 6.50 radians per second. These results imply that a SAS loop that was more responsive at the larger amplitudes would reduce the PIO tendency.
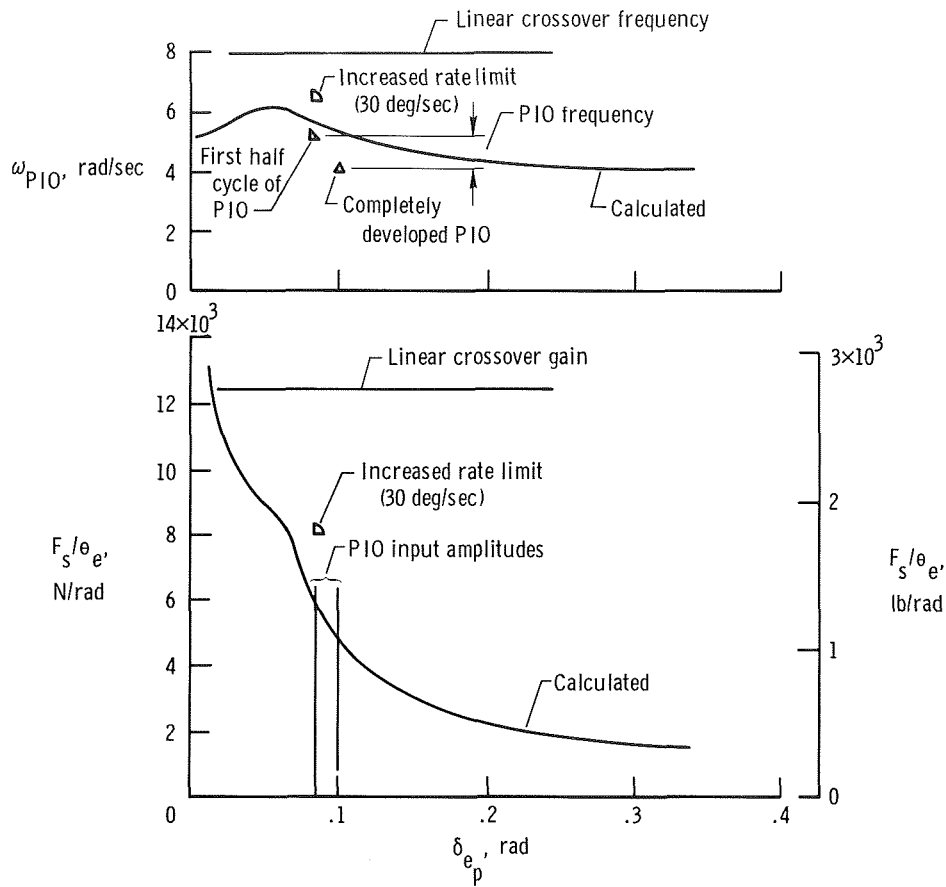

Figure 15. *PIO frequency and minimum pilot gain required for PIO versus input amplitude for* $\left(\dfrac{\delta e_p}{F_s}\right)_{linear}$ = 0.000944 rad/N (0.0042 rad/lb).

CONCLUDING REMARKS

Two types of pilot-induced oscillation (PIO) conditions were encountered during flight tests on the YF-12 airplane. To analyze the problem, studies were conducted using an analog simulator, ground tests, and linear and nonlinear calculations.

A small-amplitude PIO tendency near a frequency of 1 cycle per second existed when the pilot gain was high during refueling. The demanding nature of the control

task and the response characteristics of the airplane (short-period poles), coupled with structural bending (zeros), resulted in a continuous but small control input type of PIO. The structural flexing of the airplane, predominantly the first bending mode, was apparent to the pilot and caused him some concern at first after a disturbance; however, he avoided controlling continuously in or out of phase with the first bending mode response (2.5 cycles per second). During the early portion of refueling or at the lightweight condition, this PIO was only a minor annoyance.

A large-amplitude ($-1g$ to $3g$) and potentially more serious PIO tendency is caused by SAS rate and position saturation, which in turn cause phase lag and less amplitude attenuation. These nonlinearities can reduce the pilot gain required to sustain a PIO by more than 50 percent. SAS rate limits are more detrimental than position limits. The pilot normally does not make inputs large enough to cause saturation, so this situation is unusual. However, it can be initiated by an unexpected disturbance like a faulty trim command.

Flight Research Center
National Aeronautics and Space Administration
Edwards, Calif., December 11, 1974

APPENDIX A.—AIRCRAFT MODELING AND VERIFICATION

GROUND TESTS

Ground tests were conducted on the YF-12 airplane to determine its elevon, SAS, and actuator characteristics. An analog computer was tied in to the SAS to simulate the airplane's aerodynamics. Tests were conducted to determine the control inputs and SAS nonlinearities during a typical PIO condition, since such testing in flight might have endangered the airplane. Briefly, the tests involved applying sinusoidal inputs to the augmentation system and control cycles and step pulses to the mechanical system.

Figure 16 describes the complete simulation. Airplane systems used in the simulation consisted of gearing, G_m; actuators and servos, $A(s)$; and feedback gain and shaping, $H(s)$. The inputs to the computer were electrical signals from the transducers on the surface actuators. The gains K_1 and K_2 are the scale factors necessary to make the signals proportional to the desired control surface input and gyro output, respectively. The computer was programed using a two-degree-of-freedom simulation. The equations of motion used are presented in appendix D. Consideration of the first bending mode was confined to its effect on the normal acceleration at the cockpit, which was displayed on a meter in the cockpit. The first bending mode dynamics data were obtained from flight tests. The stability coefficients were obtained from predictions that were adjusted to flight data for a Mach number of 0.77 and an altitude of 7620 meters (25,000 feet). Appendix D lists the actual values of these coefficients.
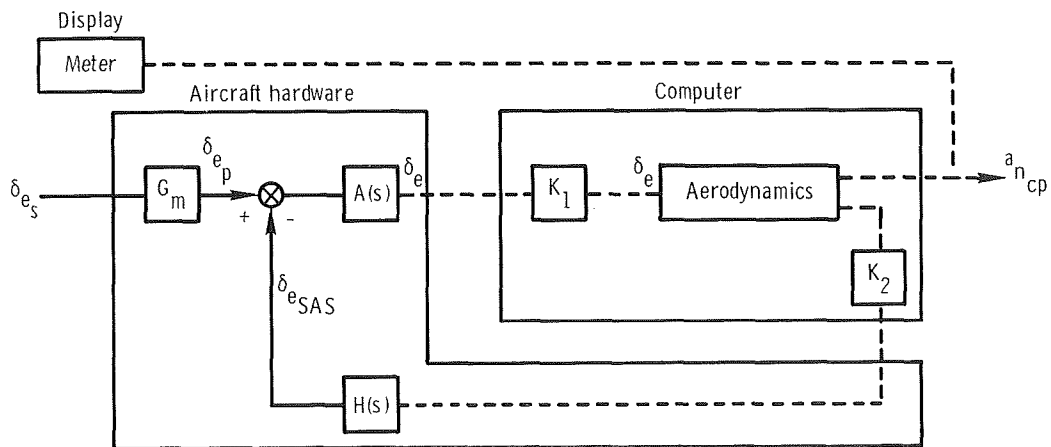

Figure 16. Description of ground test simulation.

22

Figure 17 presents typical data from these ground tests. The first part of the time history (t = 3 to 7 sec) is a control release. It was used to check the primary control response and the SAS gain. From 11 seconds on, the primary control system was pumped at a frequency near the PIO condition ($\omega \approx 4.7$ radians per second and $\Delta\delta_{e_s}$ = 17° peak to peak). Peak-to-peak excursions of 3.6g occurred in normal acceleration. The damper $\delta_{e_{SAS}}$ bottomed out at -2.5°, and rate limiting of an average value of 12.6 degrees per second was evident throughout most of the cycle.
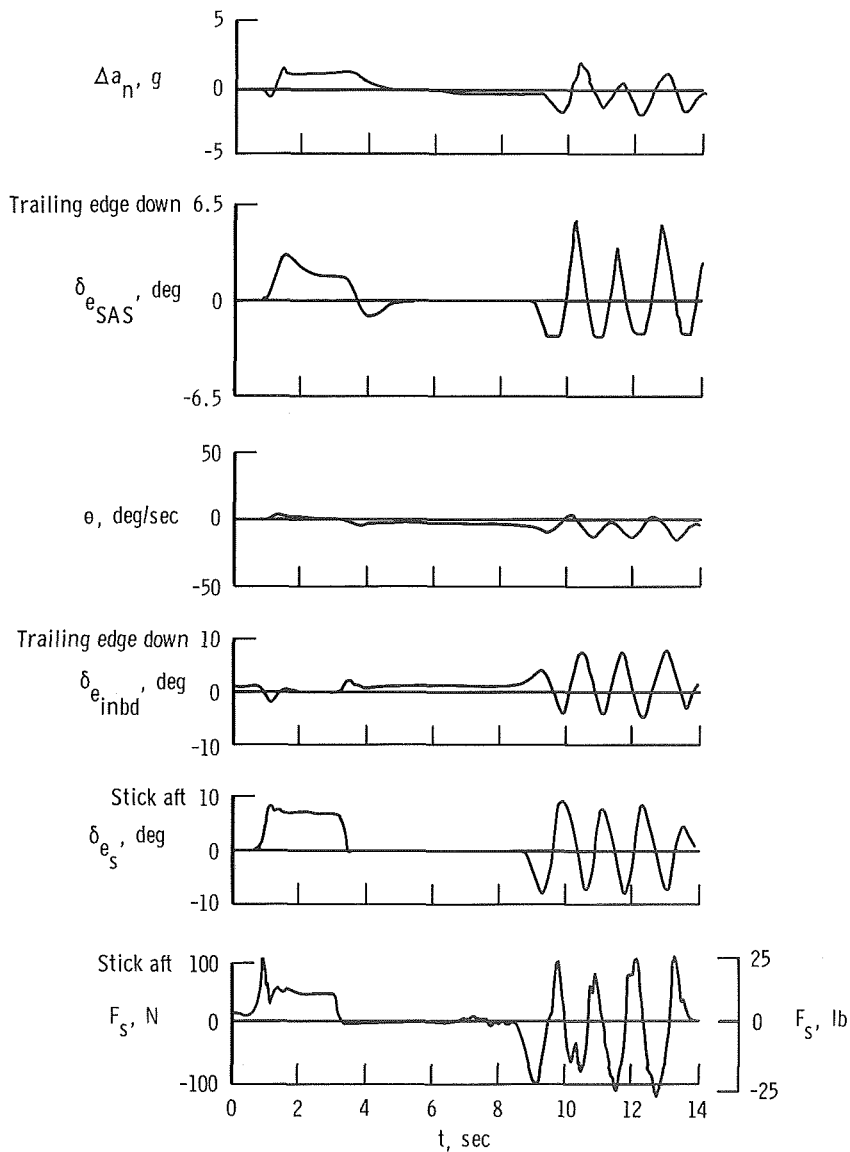
*Figure 17. Time history of control and system response obtained from ground tests simulating a PIO condition.*

23

CONTROL SYSTEM RESPONSE

The transfer functions and frequency responses of the inboard and outboard elevons to the output of the SAS servo's linear variable differential transformer (LVDT) is shown in figures 18(a) and 18(b). The amplitude ratios are fairly flat out to a frequency of 20 radians per second. At that frequency the phase difference of the inboard elevon is approximately $-25°$ and that of the outboard elevon is approximately $-100°$. The transfer functions, which were calculated by the airplane manufacturer, show good agreement with the data acquired with the actual hardware.
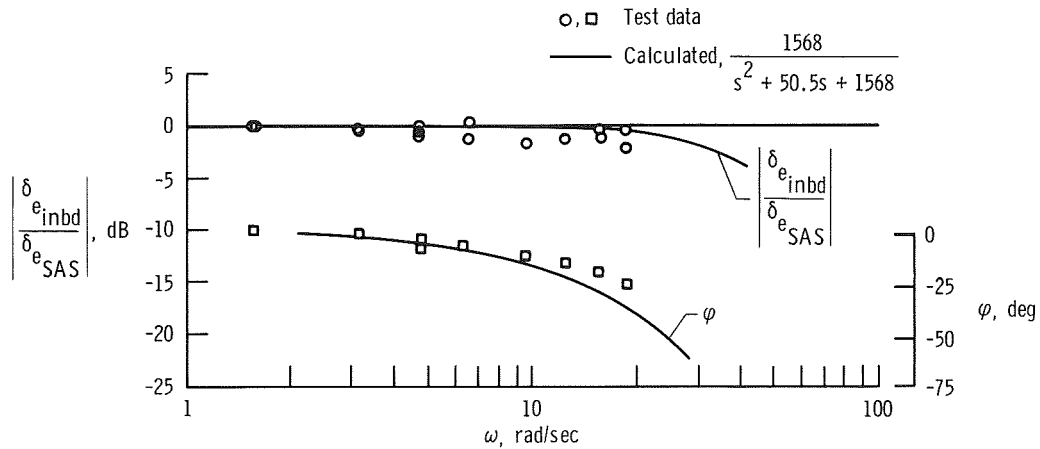
(a) Inboard elevons.
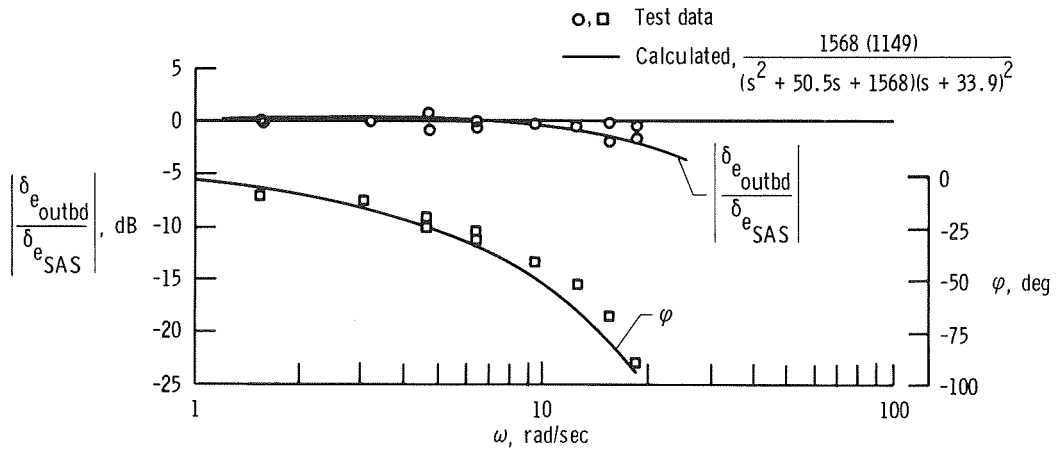
(b) Outboard elevons.

Figure 18. Frequency response of the power actuators.

To obtain better short-period closed-loop response, a lag-lead network was installed in the SAS feedback loop. The frequency response of this filter, and that of its model, $\dfrac{0.375(s + 8)}{s + 4}$, is shown in figure 19. The low order gain is approximately -2.5 decibels. With increased frequency the model data closely fit the test data. Above 12 radians per second, the dynamic characteristics of the servo were subtracted from the test data, as shown in the figure.
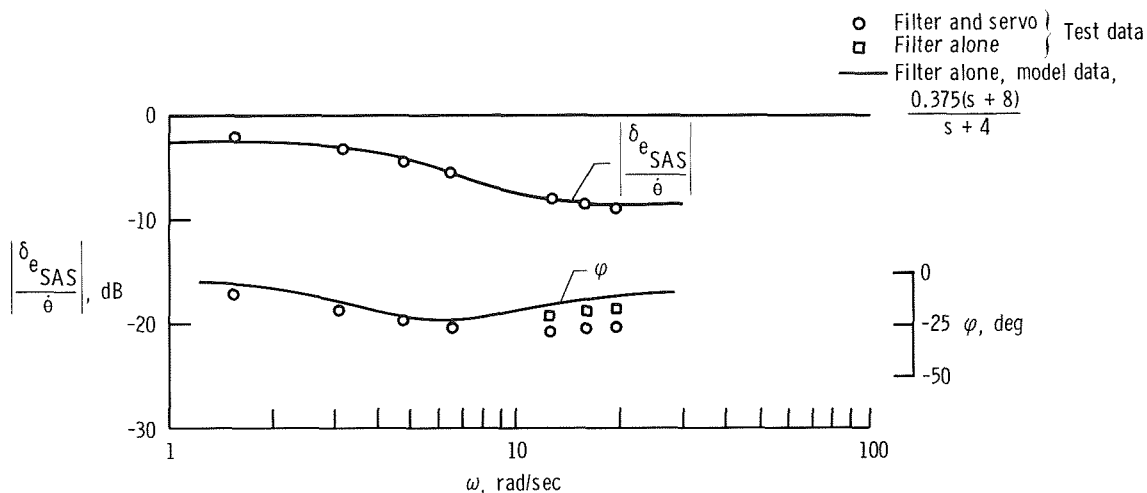

Figure 19. Frequency response of the lag-lead filter.

SIMULATOR STUDY

To acquire further evidence of the PIO problems, an analog computer was programed to simulate the control system and the airplane's aerodynamics. The mechanization of the control system included the SAS nonlinearities position and rate limits. The airplane aerodynamics consisted of a three-degree-of-freedom mechanization. The stability derivatives for the simulation were based on flight test data. A time history typical of the results is shown in figure 20. The input to the stick, δ_{e_s}, was sinusoidal, with amplitude and frequency as the principal variables. In general, the simulation showed that a PIO could be sustained and that the severity of the PIO depended on input amplitude and frequency.

Table 1 summarizes the peak-to-peak variation of the listed parameters obtained from ground tests of the airplane and from simulator studies.

FLIGHT TESTS

Flight test data of a limited nature were also obtained. The tests consisted of the manual cycling of the mechanical controls at various frequencies and at approximately one-third the g's experienced during a fully developed PIO.
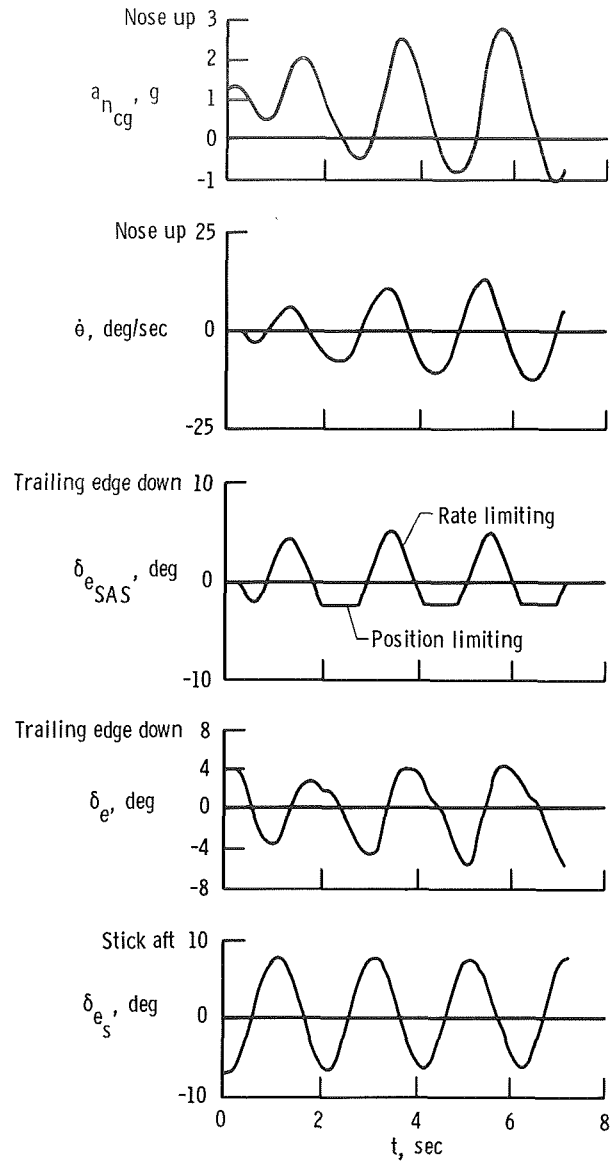
Figure 20. Analog time history with sinusoidal control input typical of a PIO.

The time history (fig. 21) indicates that nonlinearities are reached in the control system even under these restricted conditions. The data show that the damper bottoms out near $-2.5°$ at low frequencies ($f \approx 0.50$ cycle per second) and rate limits at approximately 15 degrees per second at slightly higher frequencies ($f \approx 1.25$ cycles per second).
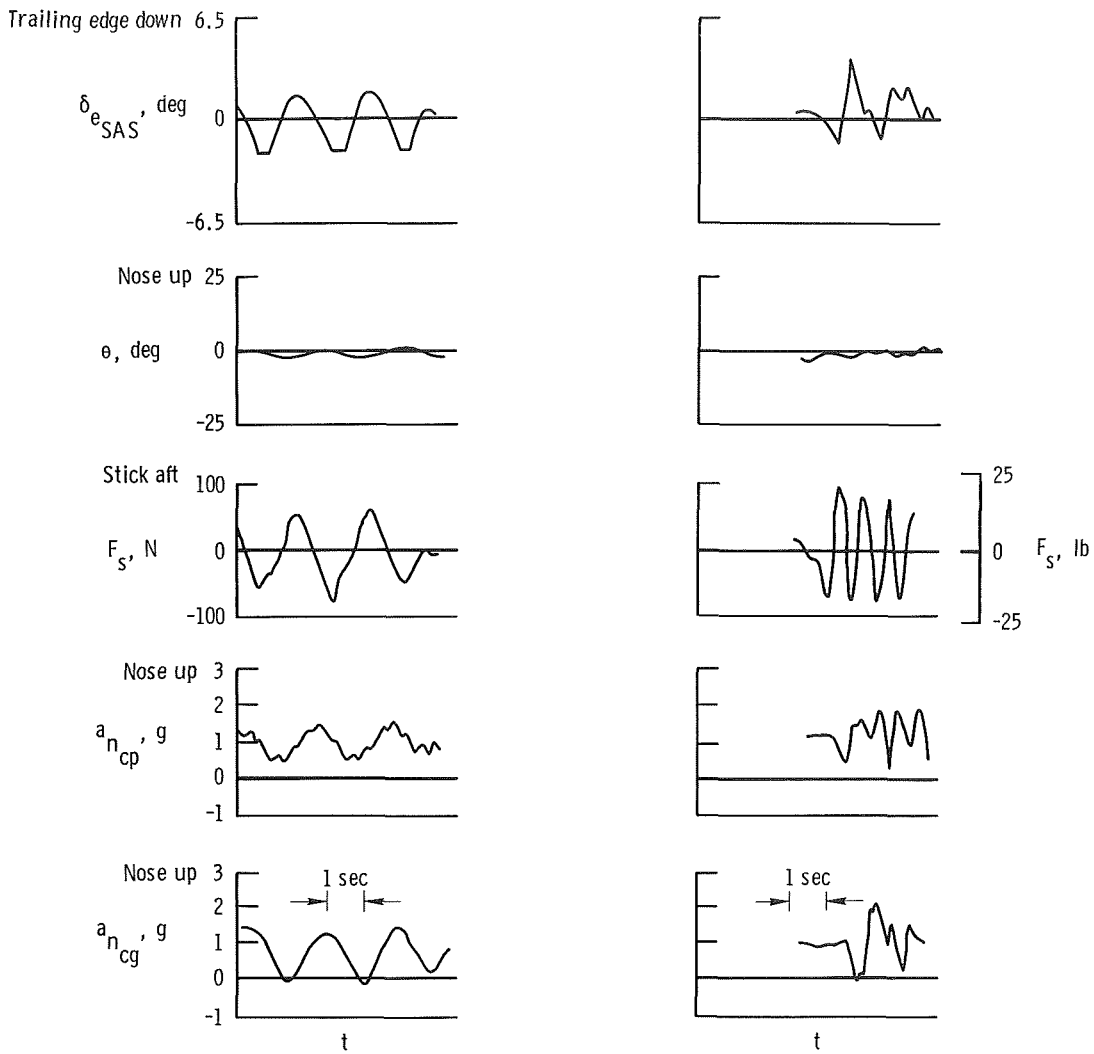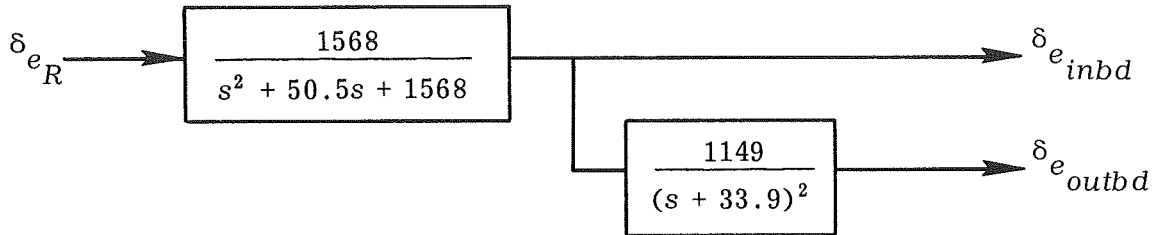
(a) Damper position limiting, f ≈ 0.50 cps.

(b) Damper rate limiting, f ≈ 1.25 cps.

Figure 21. In-flight time history. Intentional control cycling at refueling flight conditions.

The longitudinal control of the YF-12 airplane is provided by four segmented elevon surfaces that are faired into the trailing edge of the wing. An output from the inboard set of elevon actuators mechanically positions the outboard set. The diagram below is representative of the mechanical flow and transfer functions for the actuators on either side of the airplane.

$$\delta_{e_R} \longrightarrow \boxed{\frac{1568}{s^2 + 50.5s + 1568}} \longrightarrow \delta_{e_{inbd}}$$
$$\boxed{\frac{1149}{(s + 33.9)^2}} \longrightarrow \delta_{e_{outbd}}$$

Control power is the product of control effectiveness and surface deflection, as follows:

$$M = M_{\delta_e} \delta_e$$

Elevon effectiveness is less on the inboard side than on the outboard side at the particular flight condition of interest ($M_n = 0.77$, $h_p = 7620$ m (25,000 ft)):

$$\frac{C_{m_{\delta_{e_{inbd}}}}}{C_{m_{\delta_e}}} = 0.45 \text{ and } \frac{C_{m_{\delta_{e_{outbd}}}}}{C_{m_{\delta_e}}} = 0.55. \text{ Therefore, } M_{\delta_e} \text{ is simply}$$

$$M_{\delta_e} = M_{\delta_{e_{inbd}}} + M_{\delta_{e_{outbd}}}$$

The equivalent control power would be given by

$$M = M_{\delta_e} \left(0.45\delta_{e_{inbd}} + 0.55\delta_{e_{outbd}} \right)$$

where the difference in effectiveness is apportioned to the surface deflection. Substituting the transfer functions for $\delta_{e_{inbd}}$ and $\delta_{e_{outbd}}$ gives

$$M_{\delta_e} \left(\frac{\delta_e}{\delta_{e_R}} \right) = M_{\delta_e} \left[\frac{(0.45)(1568)}{s^2 + 50.5s + 1568} + \frac{(0.55)(1568)(1149)}{(s^2 + 50.5s + 1568)(s + 33.9)^2} \right]$$

By combining both transfer functions, an equivalent fourth-order description results:

$$\frac{\delta_e}{\delta_{e_R}} = \frac{705.6 \ (s^2 + 67.8s + 2553.54)}{(s^2 + 50.5s + 1568)(s + 33.9)^2} \tag{B1}$$

In factored form,

$$\frac{\delta_e}{\delta_{e_R}} = \frac{705.6 \ (s + 33.9 \pm j37.474)^2}{(s + 25.25 \pm j30.503)^2 \ (s + 33.9)^2} \tag{B2}$$

Long, slender aircraft like the YF-12 airplanes exhibit a considerable amount of structural bending throughout the flight envelope. Typically, the response of this type of airplane to a control input is somewhat modified by the bending that takes place while the structural modes are excited. Because of low damping, the longitudinal first bending mode superimposes an almost continuous small-amplitude sinusoidal response on the overall airplane's responses. For example, after a sudden input to the elevons in an upward direction (fig. 22), the aerodynamic loading on the elevons causes the wings to deflect downward. In turn, the mass near the center of gravity accelerates downward relative to the rest of the mass along the fuselage, and more so at first because of bending caused by the control input. The accelerations due to any control action are sufficient to excite the first bending mode. The initial amplitude of the first bending mode depends primarily on the abruptness and the magnitude of the control input.
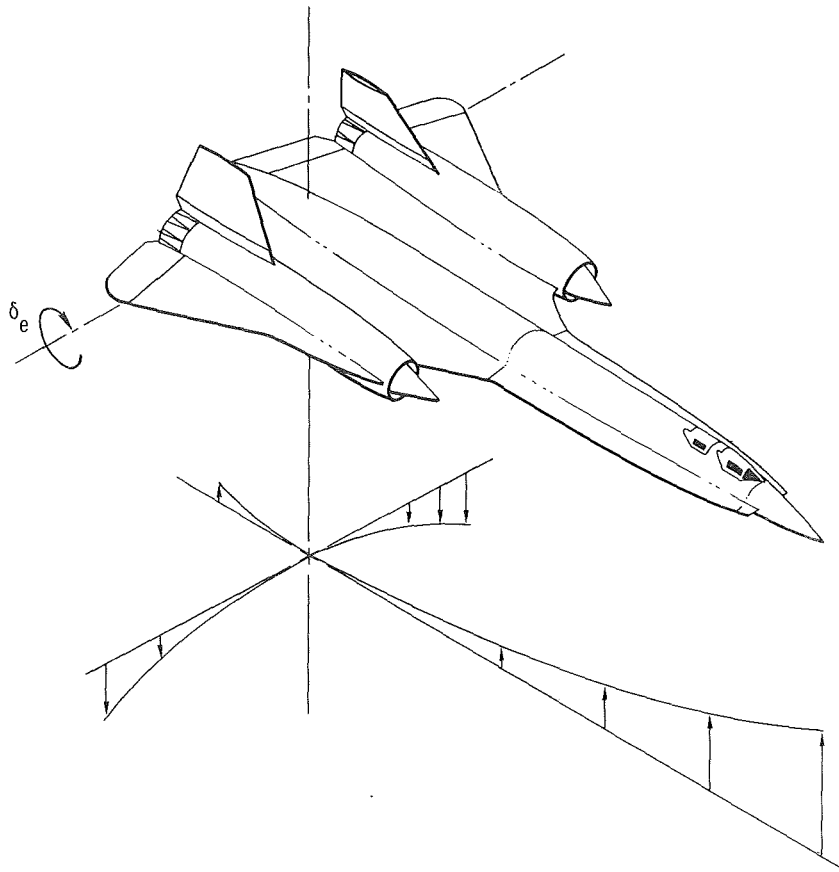
Figure 22. Bending response directions after control input.

The total pitching acceleration, $\ddot{\theta}$, at any point on the fuselage after a step input results from both the airplane's response and the additional bending of the fuselage:
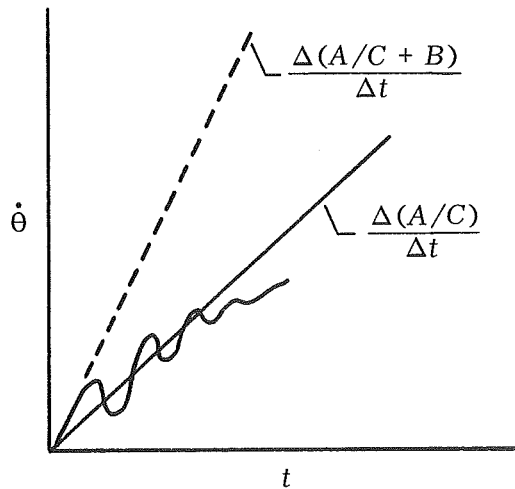
$$\ddot{\theta}_i = \frac{s\left(s + \dfrac{1}{\tau_\theta}\right) M_{\delta_e} \delta_e}{s^2 + 2\zeta_n \omega_n s + \omega_n^2} + \frac{K_B \omega_B^2 s^2 \delta_e}{s^2 + 2\zeta_B \omega_B s + \omega_B^2} \tag{C1}$$

where K_B is a constant proportional to the additional amount of bending at that location.

If the initial value theorem is applied to equation (C1), the following equation results:

$$\ddot{\theta}_i = M_{\delta_e} + K_B \omega_B^2 \tag{C2}$$

Then the initial value of $\ddot{\theta}$ is measured from a flight record or time history of $\dot{\theta}$, as follows:

The two slopes are obtained along with the bending mode natural frequency, ω_B, and bending mode damping ratio, ζ_B. The value of M_{δ_e} is usually known from wind tunnel or flight test results; therefore, enough information is available to estimate K_B.

For example, it was determined from flight data that the first bending mode frequency was 15.7 radians per second. It was also determined that $\ddot{\theta}_i$ was 1.8 for the airplane plus the first bending mode and that $\ddot{\theta}_i$ was 1.1 for the airplane alone.

31

From earlier flight test data it was determined that M_{δ_e} was approximately 6.0.

Making the substitution into equation (C1) and taking the ratio of the two different initial responses,

$$\frac{1.8}{1.1} = \frac{6.00 + K_B 246}{6.00}$$

or

$$K_{B_{\text{instrument location}}} = 0.0155 \tag{C1}$$

For this particular example, the instrument was elsewhere than in the cockpit; therefore, the mode shape was needed to determine the value of K_B at the cockpit.

Figure 5 presents the normalized bending deflection of the airplane. YF-12 bending mode data are published in reference 8. All deflections are relative to the maximum deflection, which occurs at the nose. The ratio of the slope at the cockpit to the slope at the instrumentation package is approximately 1.36, so

$$K_{B_{cp}} = 1.36 K_{B_{\text{instrument location}}} \tag{C4}$$

Therefore,

$$K_{B_{cp}} \approx 0.021$$

APPENDIX D.—EQUATIONS OF MOTION

A two-degree-of-freedom representation was considered to be adequate:

$$\dot{\gamma} = L_\alpha \alpha - \frac{g}{V} + L_{\delta_e} \delta_e \tag{D1}$$

$$\ddot{\theta} = M_{\dot{\theta}} \dot{\theta} + M_\alpha \alpha + M_{\delta_e} \delta_e \tag{D2}$$

$$\alpha = \theta - \gamma \tag{D3}$$

Taking the Laplace transform and arranging the coefficients in a matrix,

$$\begin{bmatrix} s & -L_\alpha & 0 \\ 0 & -M_\alpha & s^2 - M_{\dot{\theta}} s \\ 1 & 1 & -1 \end{bmatrix} \begin{bmatrix} \gamma \\ \alpha \\ \theta \end{bmatrix} = \begin{bmatrix} L_{\delta_e} \\ M_{\delta_e} \\ 0 \end{bmatrix} \begin{bmatrix} \delta_e \end{bmatrix}$$

from which the transfer functions can be derived as follows:

$$\frac{\theta}{\delta_e} = \frac{L_\alpha M_{\delta_e} - M_\alpha L_{\delta_e} + s M_{\delta_e}}{s \left[s^2 + \left(L_\alpha - M_{\dot{\theta}} \right) s - \left(M_{\dot{\theta}} L_\alpha + M_\alpha \right) \right]} \tag{D4}$$

$$\frac{\gamma}{\delta_e} = \frac{-L_{\delta_e} M_\alpha + \left(s^2 - M_{\dot{\theta}} s \right) L_{\delta_e} + L_\alpha M_{\delta_e}}{s \Delta} \tag{D5}$$

The first bending mode is represented by

$$\frac{\theta}{\delta_e} B = \frac{-K_B \omega_B^2}{s^2 + 2 \zeta_B \omega_B + \omega_B^2} \tag{D6}$$

The flight conditions and flight test data used for the analysis are listed below:

$g = 9.754 \text{ m/sec}^2 \ (32 \text{ ft/sec}^2)$

$h_p = 7620 \text{ m} \ (25,000 \text{ ft})$

$L_\alpha = 0.904 \text{ per sec}$

$L_{\delta_e} = 0.180 \text{ per sec}$

$M_n = 0.77$

$M_\alpha = -3.486 \text{ per sec}^2$

$M_{\delta_e} = -6.084 \text{ per sec}^2$

$M_{\dot\theta} = -0.609 \text{ per sec}$

$V = 239 \text{ m/sec} \ (786 \text{ ft/sec})$

From bending mode data and calculations (appendix C),

$$K_B = 0.021$$

$$\omega_B = 15.7 \text{ rad/sec}$$

$$\zeta_B = 0.05$$

For these flight conditions, the transfer functions become approximately

$$\frac{\theta}{\delta_e} \approx \frac{-6.00(s + 0.8)}{s(s^2 + 1.50s + 4.00)} \tag{D7}$$

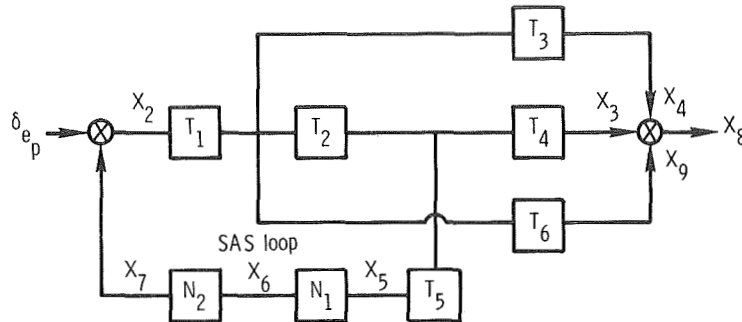$$\frac{\gamma}{\delta_e} \approx \frac{0.180(s^2 + 0.60s - 27)}{s(s^2 + 1.50s + 4.00)} \tag{D8}$$

and

$$\frac{\theta}{\delta_{e_{cp}}} B = \frac{-5.15}{s^2 + 1.57s + 246} \tag{D9}$$

APPENDIX E.—BASIC ANALYSIS AND COMPUTATIONAL PROCEDURE

The following flow diagram represents the YF-12 airplane's basic control system, aerodynamics, and structural dynamics.

In this diagram, δ_{e_p} is the input commanded by the pilot and sums with the damper feedback signal, X_7. In the SAS loop a lag-lead filter, T_5, is implemented in addition to the damper rate limits, N_1, and position limits, N_2. The output parameter, X_8, depends on the transfer function: T_1, T_2, T_3, and so forth.

This representation can be used for both linear and nonlinear calculations. For linear calculations, N_1 and N_2 equal 1. For nonlinear calculations, the existing amount of rate limiting and position limiting is assigned to N_1 and N_2, respectively.

To obtain a frequency response, various values are assumed and assigned to $X_2(A,\omega)$, a vector that is a function of both frequency and amplitude. Then the vector signal is traced for each calculation. The phase and amplitude of each successive vector are noted through each block and summation junction until an input-output vector relationship is determined.

The following logic was programed on a digital computer:

$s = j\omega$, where ω is variable

$X_2 \qquad$ variable

$X_3 = T_1 T_2 T_4 X_2$

$X_4 = T_1 T_3 X_2$

$X_5 = T_1 T_2 T_5 X_2$

$X_6 = X_5 s \leq N_1$

$X_7 = \dfrac{X_6}{s} \leq N_2$

$X_8 = X_3 + X_4 + X_9$

$X_9 = T_1 T_6 X_2$

$\delta_{e_p} = X_2 + X_7$

This makes $\dfrac{X_8}{\delta_{e_p}}$ a function of X_2 and ω. The quantity X_8 can be any one of the parameters θ, $\dot\theta$, $\ddot\theta$, or a_n, depending on the transfer functions T_3, T_6, and T_4 where

N_1 rate limit, 15 degrees per second or 12.6 degrees per second

N_2 position limit, $2.5°$ or $6.5°$

T_1 actuators, $\dfrac{705.6(s^2 + 67.8s + 2553.5)}{(s^2 + 50.5s + 1568)(s + 33.9)^2}$

$T_2 = \dfrac{\dot\theta}{\delta_e} = \dfrac{-6.00(s + 0.8)}{s^2 + 1.50s + 4.00}$

T_5 shaping, $\dfrac{0.375(s + 8)}{s + 4}$

For a_n/δ_e at the center of gravity,

$$T_3 \approx 0$$

$$T_4 \approx 0$$

$$T_6 = \frac{\dot\gamma}{\delta_e}\frac{V}{g} = \frac{4.5(s^2 + 0.60s - 27)}{s^2 + 1.50s + 4.00}$$

For θ/δ_e at the cockpit,

$$T_3 = \frac{\theta}{\delta_e}B = \frac{-5.15}{s^2 + 1.57s + 246}$$

$$T_4 = \frac{1}{s}$$

$$T_6 = 0$$

The feel system of a fighter airplane is usually represented by a second-order system (ref. 10). However, flight data were available at the PIO frequency that indicated that there was a hysteresis loop in the function. It seemed reasonable to assume that the pilot applied a force to provide the desired stick displacement; therefore, stick position, δ_{e_s}, was considered to be the output. Figure 23 presents data
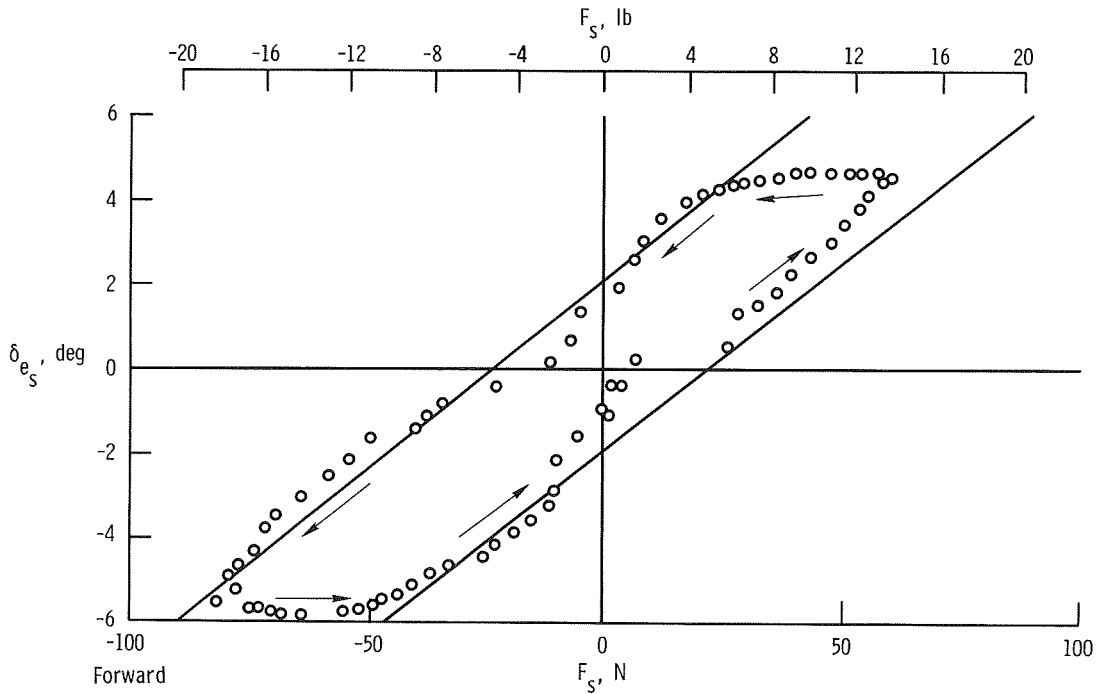

Figure 23. Stick position versus stick force. Flight data; f = 0.5 cps; $\dfrac{\Delta\delta_{e_s}}{\Delta F_s}$ = 0.0863 deg/N (0.384 deg/lb).

typical of stick position as a function of stick force. The hysteresis loop shown by the straight lines was considered to be representative of the feel system. The breakout force was approximately 22.24 newtons (5 pounds). The gradient $\dfrac{\Delta\delta_{e_s}}{\Delta F_s}$ was approximately 0.0863 degree per newton (0.384 degree per pound). Figure 24 shows the describing function for hysteresis adapted from reference 11. With this describing function and faired data from figure 23, the feel system was represented as a function of stick output, δ_{e_s}. To account for gearing change with stick position, the following cubic equation was used:

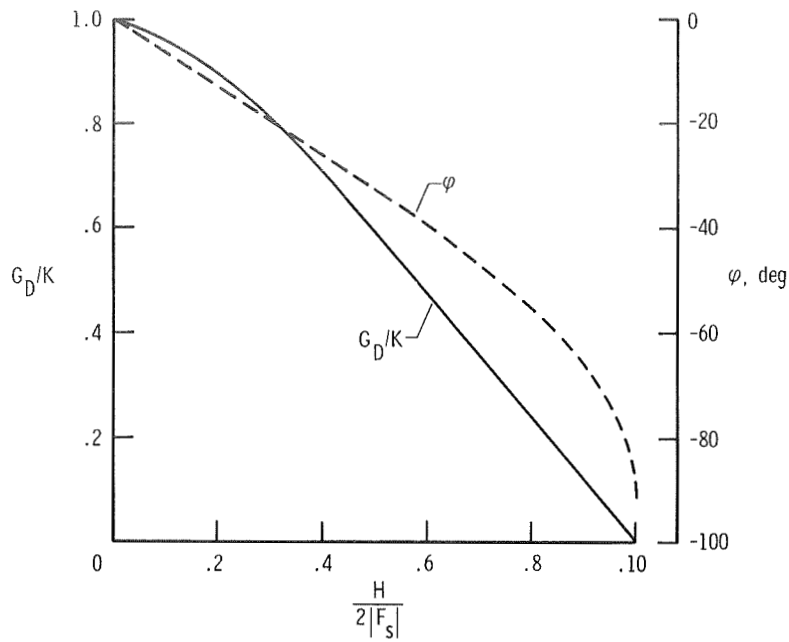$$\delta_{e_p} = f\left(\delta_{e_s}\right) = 0.002788\delta_{e_s}^{3} + 0.45556\delta_{e_s} \tag{F1}$$

Figure 24. Hysteresis-describing function (adapted from ref. 11).

Figure 25 compares the results of this equation with experimental data from a preflight control cycle. The data show some hysteresis due to the actuator. This hysteresis was accounted for in the digital computer program's description of the
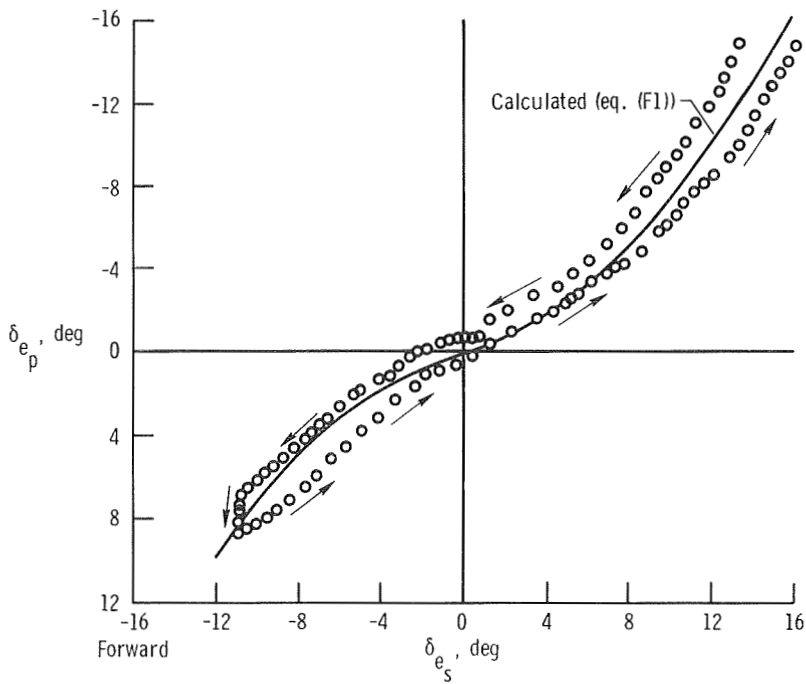

Figure 25. Mechanical gearing. Preflight control cycle (SAS off).

airframe plus augmentation system. The cascade combination of feel system plus the gearing is shown in figure 26. The amplitude and phase are presented in terms of output amplitude. This is actually the input command, δ_{e_p}, from the pilot to the actuators (fig. 26). As expected at low amplitudes, the phase difference is large and the amplitude ratio of $\dfrac{\delta_{e_p}}{F_s}$ is low. With increasing amplitudes of δ_{e_p}, the phase difference decreases and the amplitude ratio increases.
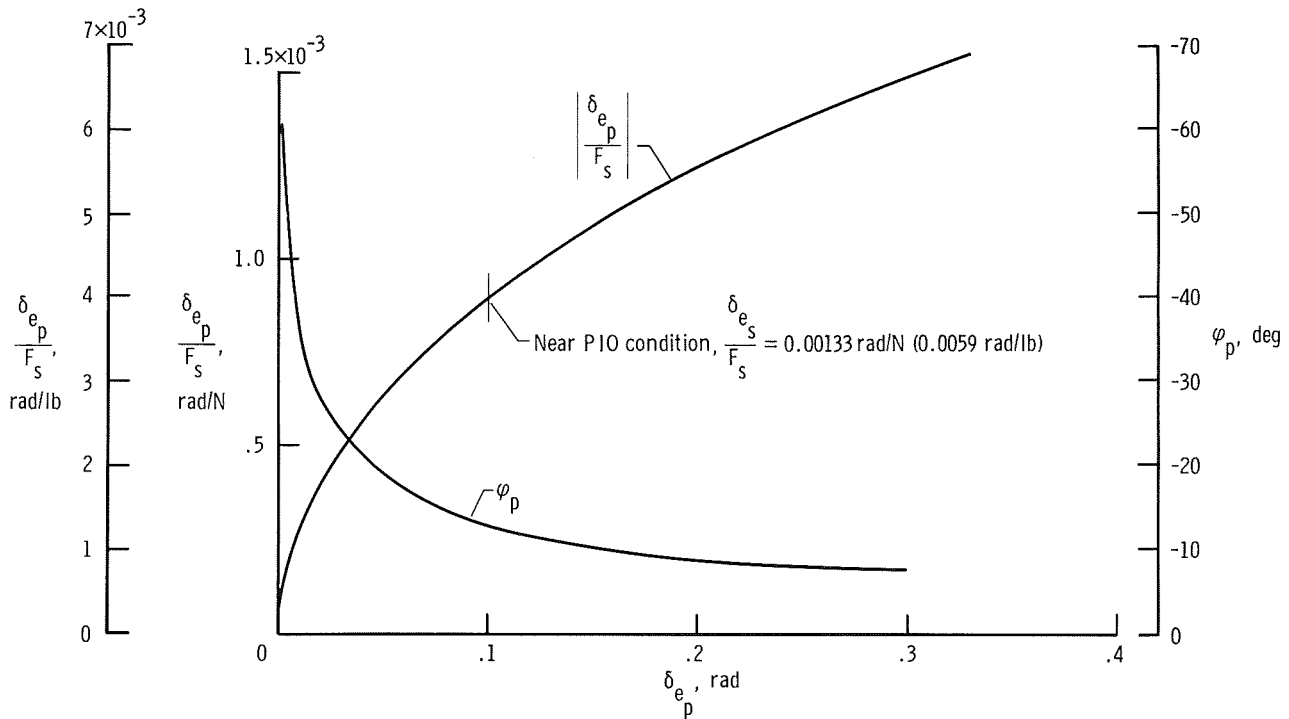

Figure 26. Amplitude and phase characteristics of the feel system.

$$\left(\frac{\delta_{e_s}}{F_s}\right)_{linear} = 0.0015 \; rad/N \; (0.0067 \; rad/lb).$$

REFERENCES

1. Ashkenas, Irving L.; Jex, Henry R.; and McRuer, Duane T.: Pilot-Induced Oscillations: Their Cause and Analysis. STI TR-239-2, Systems Technology, Inc., June 20, 1964.

2. Phillips, William H.; Brown, B. Porter; and Matthews, James T., Jr.: Review and Investigation of Unsatisfactory Control Characteristics Involving Instability of Pilot-Airplane Combination and Methods for Predicting These Difficulties From Ground Tests. NACA TN 4064, 1957.

3. Jex, H. R.: Summary of T-38A PIO Analyses. Tech. Rep. No. 239-1, Systems Technology, Inc., Jan. 25, 1963.

4. Johnson, Harold I.: Flight Investigation To Improve the Dynamic Longitudinal Stability and Control-Feel Characteristics of the P-63A-1 Airplane (AAF No. 42-68889) With Closely Balanced Experimental Elevators. NACA WR L-730, 1946. (Formerly NACA MR L6E20.)

5. Finch, Thomas W.; and Matranga, Gene J.: Launch, Low-Speed, and Landing Characteristics Determined From the First Flight of the North American X-15 Research Airplane. NASA TM X-195, 1959.

6. Mechtly, E. A.: The International System of Units - Physical Constants and Conversion Factors. Second Revision. NASA SP-7012, 1973.

7. Gilyard, Glenn B.; Berry, Donald T.; and Belte, Daumants: Analysis of a Lateral-Directional Airframe/Propulsion System Interaction. NASA TM X-2829, 1973

8. Wilson, Ronald J.; Cazier, Frank W., Jr.; and Larson, Richard R.: Results of Ground Vibration Tests on a YF-12 Airplane. NASA TM X-2880, 1973.

9. Jarvis, Calvin R.; Loschke, Paul C.; and Enevoldson, Einar K.: Evaluation of the Effect of a Yaw-Rate Damper on the Flying Qualities of a Light Twin-Engine Airplane. NASA TN D-5890, 1970.

10. DiFranco, Dante A.: Flight Investigation of Longitudinal Short Period Frequency Requirements and PIO Tendencies. AFFDL-TR-66-163, Air Force Flight Dynamics Lab., Wright-Patterson AFB, June 1967.

11. Grabbe, Eugene M.; Ramo, Simon; and Wooldridge, Dean E., eds.: Handbook of Automation, Computation, and Control. Volume 1 — Control Fundamentals. John Wiley & Sons, Inc., c.1958.

"The aeronautical and space activities of the United States shall be conducted so as to contribute . . . to the expansion of human knowledge of phenomena in the atmosphere and space. The Administration shall provide for the widest practicable and appropriate dissemination of information concerning its activities and the results thereof."
—NATIONAL AERONAUTICS AND SPACE ACT OF 1958

NASA SCIENTIFIC AND TECHNICAL PUBLICATIONS

TECHNICAL REPORTS: Scientific and technical information considered important, complete, and a lasting contribution to existing knowledge.

TECHNICAL NOTES: Information less broad in scope but nevertheless of importance as a contribution to existing knowledge.

TECHNICAL MEMORANDUMS: Information receiving limited distribution because of preliminary data, security classification, or other reasons. Also includes conference proceedings with either limited or unlimited distribution.

CONTRACTOR REPORTS: Scientific and technical information generated under a NASA contract or grant and considered an important contribution to existing knowledge.

TECHNICAL TRANSLATIONS: Information published in a foreign language considered to merit NASA distribution in English.

SPECIAL PUBLICATIONS: Information derived from or of value to NASA activities. Publications include final reports of major projects, monographs, data compilations, handbooks, sourcebooks, and special bibliographies.

TECHNOLOGY UTILIZATION PUBLICATIONS: Information on technology used by NASA that may be of particular interest in commercial and other non-aerospace applications. Publications include Tech Briefs, Technology Utilization Reports and Technology Surveys.

Details on the availability of these publications may be obtained from:

SCIENTIFIC AND TECHNICAL INFORMATION OFFICE

NATIONAL AERONAUTICS AND SPACE ADMINISTRATION
Washington, D.C. 20546